國立臺灣大學理學院心理學研究所

碩士論文

Graduate Institute of Psychology

College of Science

National Taiwan University

Master Thesis

從「不可能」到「可能」：探討三維不可能物體的知覺推論與神經活動

From “Impossible” to “Possible”: Investigating Perceptual Inference and Neural Activity on 3D Impossible Objects

謝依眞

Yi-Chen Hsieh

指導教授：賴文崧 博士

Advisor: Wen-Sung Lai, Ph.D.

中華民國 111 年 12 月

December 2022

doi:10.6342/NTU202210143

國立台灣大學理學院心理學研究所

論文口試委員會審定書

謝依真 先生所提論文 From "Impossible" to "Possible": Investigating Perceptual Inference and Neural Activity on 3D Impossible Objects

經本委員會審議， 符合 碩 士學位標準， 特此證明。

論文考試委員會

主席 鄭仁坤

委員 張仁俊 曾祥非

黃榮村 鄭仁坤

賴文琦

指導教授：賴文琦

所 主 任：周泰立

中華民國 111 年 07 月 04 日

doi:10.6342/NTU202210143

誌謝

待在台大求學的日子接近尾聲，大學加上碩士研究生的學習階段即將結束，七年多來在台大心理系的生活將要畫下句點。在大學建構的基石，再經歷研究所的磨礪，得以產出成果。碩士畢業論文完稿後，回首一切搜尋、建立、執行、分析、討論的過程，歷程中收到許多的關懷及幫助，欲以此致詞表達我最誠摯的謝意。

首要感謝我的指導老師賴文崧教授，非常感謝賴老師給了我在實驗室學習深造的機會，在論文的選題、設計與執行中，賴老師都給予我極大的空間與鼓勵，並提供給我豐富的資源，讓我得以無後顧之憂地完成實驗並完成論文。在研究的過程中，有任何需要時，賴老師都會在百忙之中抽出空來與我進行討論，提出許多中肯的指導意見，使我在研究和寫作過程中不致迷失方向。賴老師對待科學研究的態度影響我許多，也激勵著我以更加嚴謹且端正的態度進行學術研究，我將永遠銘記賴老師的諄諄教誨。

謝謝日本明治大學工程數學專業的杉原厚吉教授及國立故宮博物院的蔡慶良博士。謝謝杉原教授慷慨提供其畢生之作，使我有這麼多不可能物體作為刺激材料，成為我論文的靈魂。謝謝蔡慶良博士獨到的眼光及見解，使不可能物體在我論文的使用得以有所發揮。謝謝兩位非心理學專業的老師的加持，讓我的論文更具別樣風采。

謝謝台大醫院謝明憲醫師、乃瑩學姊，讓我能夠有機會學習如何施作腦波實驗，讓我從零開始，到現在可以獨立施作執行實驗。謝謝長庚大學職能治療系陳柏伃老師，謝謝老師讓我在實驗室跟著學習基礎的腦波分析方法，為我鋪

doi:10.6342/NTU202210143

好往後進階資料分析的基礎。

謝謝黃榮村老師、曾祥非老師、鄭仕坤老師、謝伯讓老師，承蒙惠允擔任本人學位論文的口試委員，使我的論文在收尾階段得以有所提升，也給我許多珍貴的建議，讓我能將論文更加完好的呈現，並給予我後續研究上一些新的想法及可以調整的方向，真的非常感謝老師們的鼎力相助。

謝謝整合神經科學與行為學實驗室(LINE Lab)的同仁們，在每週實驗室會議時竭盡所能地參與討論，讓我的研究日益完善。不僅如此，也給了我精神上的支持，在 417 跟大家談天的日子是我研究所生活的一大調劑，很高興能在我的碩士生涯中結識大家，能在這樣一個團隊中度過真的很榮幸。特別謝謝虹翔學長，謝謝學長在我茫然的時候給予我許多寶貴的建議，也提供給我所有我需要的，給我的研究之路帶來極大的幫助，讓我可以順利完成論文，也學習到更多往後我所需具備的技能及軟實力，真的非常謝謝能夠有學長走在我前面。

謝謝洛涵，跟你一起聊天耍廢的時光總是過得特別快，謝謝有你陪我一起度過漫長的研究生生活。謝謝張乃有、蔡皖如，三人行延續至今，謝謝有你們在身後支持我，謝謝你們一直都在。謝謝女籃的隊友們，跟你們一起練球、比賽，真的很舒壓，謝謝有你們這群這麼單的隊友。謝謝羊咩咩們，當初接下向陽總籌，換來你們這群夥伴真的太好了，謝謝有你們相互砥礪。謝謝心理系的大家，在大學畢業後還能常常約飯、約跨年，謝謝有你們能夠互相支持。

感謝我的家人，謝謝阿母跟妹妹，因為有你們做後盾，我才能沒有顧慮的完成我想做的任何事，有你們真的很幸運，謝謝有你們作為我的家人。

最後想要謝謝我自己，還有我的偶像們。

doi:10.6342/NTU202210143

摘要

人類借助經驗比對接收到的感覺訊息，以處理眼花撩亂的世界，大腦做出的預測可加速此過程，但這樣的預測可能出現錯誤—錯覺。以往針對視錯覺相關之研究，多是以二維刺激材料進行，幾乎沒有關於三維錯覺之研究。日本數學藝術家—杉原厚吉教授，將二維錯覺轉換為獨特的三維不可能物體，使更深入的研究得以進行。藉由杉原教授提供的三維不可能物體（這些物體在鏡子前後擁有截然不同的兩個形狀），本研究以空間性向測驗挑選出 30 個物體作為刺激材料，並將物體拍攝成一系列之刺激影片，建立「鏡像辨識作業」及「知覺推論作業」，搭配腦電波來同步量測及探討其創造之不可能物體形成的預測錯誤之知覺訊號，以及知覺推論歷程的神經活動。根據鏡像辨識作業，當非預期的鏡像呈現時，腦波事件關聯電位及事件關聯頻譜震盪分析皆顯示可能的預測錯誤之相關信號，並且有類似情緒反應之晚期正電位。同時透過多元模式分析，知覺推論不同物體時的腦神經動態可以被分辨，且物體的複雜程度亦可影響其效果，而透過事件關聯電位分析得以進一步確認相關腦波成分分布。本論文以探索性之研究，強調錯覺相關知覺歷程之神經動態，開啟往後進一步探討三維錯覺實證研究之路。

關鍵詞：三維不可能物體、錯覺、預測錯誤、知覺推論、腦電波、事件關聯電位、事件關聯頻譜震盪、多元模式分析

doi:10.6342/NTU202210143

From “Impossible” to “Possible”: Investigating Perceptual Inference and Neural Activity on 3D Impossible Objects

Yi-Chen Hsieh

Abstract

We lean on matching sensory inputs with experiences to process the dazzling world. Our brain tends to make predictions to facilitate this processing; however, the brain could commit errors—illusions. In contrast to the various research on 2-dimensional (2D) optical illusory stimuli, there is hardly any empirical neural investigation of 3D authentic misrepresentation. Professor Kokichi Sugihara, a Japanese mathematician as well as artist, has turned the 2D illusions into 3D impossible objects, which allowed in-depth investigation into these intriguing perceptual field. Professor Kokichi Sugihara kindly provided the authentic 3D impossible objects whose appearance from the front view is incongruent with their reflection in the mirror. After conducting a spatial aptitude test to select 30 suitable 3D objects for this study, I created a set of video clips of authentic 3D impossible objects. Through the designed tasks: the peekaboo task and the perceptual inference task, I investigated the incongruent perceptions and the neural dynamics underlying the inference process of 3D illusion with the electroencephalogram (EEG). The result of the peekaboo task revealed significant differences between impossible objects and their counterparts in the time segment after the expected or unexpected sensory data inputs, which reflected the potential predictive error signals and also possible affective arousal. Applying multivariate pattern analysis (MVPA) to simultaneous EEG recordings, my result indicated that the impossible objects can be discriminated from the possible ones in the perceptual inference task, even between two

doi:10.6342/NTU202210143

configuration levels. With these exploratory results, this study highlights the neural dynamics underlying illusory-like perception and sheds the light on the sensory processing of these unique 3D impossible objects.

Keywords: 3D impossible object, illusion, prediction error, perceptual inference, electroencephalogram (EEG), event-related potential (ERP), event-related spectral perturbation (ERSP), multivariate pattern analysis (MVPA)

doi:10.6342/NTU202210143

Table of Contents

doi:10.6342/NTU202210143

doi:10.6342/NTU202210143

Chapter 1. General Introduction

1.1. Illusory Perception

The world we live in is not beyond imagine, this allows us to handle various events. With the build-in internal models, we can make use of previous experience and newly input to face this predictable world. As “anticipatory systems” (Alink, Schwiedrzik, Kohler, Singer, & Muckli, 2010), we construct predictive models to make sense of incoming information effectively. The brain in between act as a “prediction machine” (Anderson, Dakin, & Rees, 2009) that generate top-down expectations and match wide-ranging sensory inputs in order to facilitate sensory processing. However, there are some consequences of predictive perception, and one of the famous examples is an illusion.

It may be fun to perceive illusions, as they usually provide us with surprising experiences that are out of our expectations, but the understanding of how they work is even more stimulating and sustainable. Conventionally, they are regarded as “failures” or “biases” of perception and can be therefore used to probe the limits and capacity of our perceptual systems (Coren, 2012). Instead of referring to them as failures, on the other hand, Bayesian considerations posit that illusions are still optimal perceptions (Friston, 2005, 2010; Friston, Kilner, & Harrison, 2006). The main point made by this line of research is that illusory percepts occur when the individual encounters stimuli which link to vague or multiple prior beliefs that are incongruent with current sensory input. These kinds of stimuli are ambiguous and could be explained by different underlying causes. To reconcile this ambiguity, under the framework of Bayesian inference, the perceptual system would compute the most likely explanation (i.e., the posterior probability) by combining all the prior beliefs about the hidden causes with the

doi:10.6342/NTU202210143

existing sensory input. The results are not just illusions but are also optimal percepts in the given situations.

The idea above has been supported by several studies (e.g., Purves, Shimpi, & Lotto, 1999), however, the empirical investigation of its neurobiological foundation is still scarce. The scarcity was mainly due to the limitation of available stimuli, most of which are 2-dimensional (2D) optical illusory figures (e.g., Douglas, 2017; Freud, Ganel, & Avidan, 2015; Friedman & Cycowicz, 2006; Shigemura, Yoshino, Kobayashi, Takahashi, & Nomura, 2004; Wu, Li, Zhanga, & Qiu, 2011). This limitation restricts the experimental design of illusory related study and confines the illusory related study to 2D illusions. Thanks to Professor Kokichi Sugihara, a world-famous Japanese mathematician as well as artist, has turned the well-explored 2D illusions into 3D impossible objects, which allowed in-depth investigation into these 3D illusions. Taking advantage of Professor Kokichi Sugihara's collections, I designed a series of tasks to explore the 3D illusory and incongruent perceptions with electroencephalogram (EEG).

1.2. Turning Professor Kokichi Sugihara's Unique Visual Arts into Experimental Stimuli to Study Perceptual Process

Dr. Sugihara created a series of 3D objects, which seem to violate optical physics and realize the "anomalous mirror symmetry" (Sugihara, 2016a). I adopt the third to sixth generations of 3D impossible objects which created and named by Kokichi Sugihara (Sugihara, 2015, 2016a, 2016b, 2018a, 2018b). They are all authentic 3D structures with a unique feature: their appearance from the front view is so incongruent with their reflection in the mirror that the viewer is hard to believe that they are the same objects. This gives rise to an opportunity of disentangling the two-component

doi:10.6342/NTU202210143

processes of Bayesian perceptual inference: the integration of prior belief with sensory input and the perceptual inference (Friston et al., 2006).

Specifically, as the peekaboo-like scenario demonstrated by Sugihara, when individuals are presented with a 3D impossible object with a covered mirror behind it, they would formulate a prediction on the configuration of the object (i.e., prior belief) based on its front-view appearance. Later, at the time the mirror is uncovered to show the reflection of the object to the individuals, a strong prediction error (PE) of the configuration would occur as the perception system of the individuals cannot integrate the prior belief with such incongruent sensory inputs. Then, the object would be rotated to show its whole configuration, and the perceptual system of the individuals could thus reconcile the incongruent percepts and make an inference on why the object has dual appearances. The time courses PE signaling and perceptual inference are separated in this kind of setting, which were modified as the experimental tasks of this study.

1.3. Sensory Prediction Error Signals

One of the main goals of the study is characterizing the PE signaling elicited by the incongruence between the front-view appearance of the 3D impossible objects and their alternative appearance in the mirror. Several studies have tried to provide evidence for sensory PE signals, but these studies rarely included the sensory illusory perceptual scene. Most of these studies emphasized on repetition and expectation suppression or pattern-violation (e.g., Wacongne Labyt, van Wassenhove, Bekinschtein, Naccache, Dehaene, 2011; Stefanics, Kremlácek, Czigler, 2014; Symonds, Lee, Kohn, Schwartz, Witkowski, & Sussman, 2017).

The present study chose to use electroencephalogram (EEG), which is known as a

doi:10.6342/NTU202210143

non-invasive measure of brain activities with high temporal resolution (Luck, 2014), to identify the sensory PE signals. Event-related potentials (ERP), which can be elicited by a wide variety of sensory (Sur & Sinha, 2009), were captured to find the neural activity related to illusory and unexpected sensory inputs which might represent the sensory PE. Among related EEG experiments, the feedback-related negativity (FRN), an ERP component, is usually used in the studies of reinforcement learning (RL) and decision making to reflect the signaling of reward prediction error (Amiez, Joseph, & Procyk, 2005; Mars, Coles, Grol, Holroyd, Nieuwenhuis, Hulstijn, & Toni, 2005; Miltner, Braun, & Coles, 1997; Walsh & Anderson, 2012). Its counterpart – error-related negativity (ERN) – is also been reported to reflect the activity of a generic outcome monitoring system (Boksem & De Cremer, 2010). While the task in this present study is not in the scenario of RL task, the task is still possible to elicit prediction error that may reflect on the component, which has been proved to encode an information prediction error (Brydevall, Bennett, & Murawski, 2018). Nevertheless, the task is far apart from other PE-related experiments, the ERP cannot be the only tool to use to establish this sensory PE signals.

While evaluating the conventional ERPs, event-related spectral perturbation (ERSP) was also conducted to measure dynamic changes in amplitude of the broad band EEG frequency spectrum (Makeig, 1993). As a time-frequency analysis method, ERSP can provide another complementary view when investigating the sensory PE signals. In addition to ERP components such as medio-frontal ERN (Gehring, Goss, Coles, Meyer, & Donchin, 1993), medio-frontal oscillatory change in theta frequency range was associated error-elicited change (Luu & Tucker, 2001). Recent evidence has also shown that feedback information is carried by alpha/beta oscillations, reflecting the bottom-up

doi:10.6342/NTU202210143

propagation of PE (Bastos et al., 2015). Although all these sensory-related experiments discovered some evidence of sensory PE signals, the exact frequency bands and relative timing of the sensory PE signals evoked by distinct sensory inputs remained unclear. The present study with the distinctive stimuli created by Dr. Sugihara would be another breakthrough of the investigation in this developing field.

1.4. Perceptual Inference

Previously, studies had indicated that the human visual system might be difficult to represent impossible 3D structure, and this illusory perception could be interpretations of contradicted sensory inputs (Deregowski & Bentley, 1987, Wu et al., 2011; Young & Deregowski, 1981). The impossible objects created by Dr. Sugihara, however, are different from the impossible 3D structure used in previous experiments. The impossible objects utilized in this study are actually “possible”, and this turn the original contradictive perception into a possible illusory perception. The perceptual inference process of this kind of illusory perception then become newfangled.

To capture the dynamics that manifest perceptual inference in this study, multivariate pattern analysis (MVPA) was applied in the study. MVPA is a spatio-temporal analysis that could base on the observed patterns of brain response in different experimental conditions to characterize them (Peters, Pfurtscheller, & Flyvbjerg, 1998), and it has gained much popularity in the field of EEG and MEG analysis in recent years. MVPA provides the chance to characterize neural dynamics over time through temporal generalization (King & Dehaene, 2014) and can further identify the unknown effects of the different conditions without channel selection in advance (Fahrenfort, Grubert, Olivers, & Eimer, 2017). These make the multivariate approach a suitable method for

doi:10.6342/NTU202210143

the analysis of the perceptual inference of 3D impossible objects, since the objects are one of a kind.

Along with MVPA, ERPs were also evaluated in the process of perceptual inference. It is essential to explore the components that might involve in this kind of illusory perceptual inference. The midline sites of EEG (i.e., Fz, FCz, Cz, CPz, Pz, Oz) were the highly concerned channels in this study, for that the communication between frontal and parietal cortices, also known as the multiple-demand network, has been reported to involve in a variety of tasks that have high demand on mental inference (for a review, see Duncan, 2010).

1.5. Research Purposes

Accordingly, I modified the peekaboo-like scenario demonstrated by Dr. Sugihara into the session 1, the peekaboo task, to explore the neural correlates for PE signaling. The sensory PE signals of the task were expected to be related to FRN- or ERN-like components, and that the effect was also expected to be verified through time-frequency analysis. The following session 2, the perceptual inference task, were carried out to explore the process of perceptual inference of 3D impossible objects. It was expected that the 3D impossible objects could be discriminated from the possible ones by the MVPA, and that the two configuration levels could also be decoded. The ERP results of the task could further confirm the divergent neural activities during the inference process. Through this protocol, I expected the neural dynamics underlying these processes would be differentiated by EEG signatures. Findings of this study shall improve our understandings of the neurobiological foundation of Bayesian perceptual inference and also the illusory-like perception.

doi:10.6342/NTU202210143

Chapter 2. Material and Methods

2.1. Participants

Forty paid participants were recruited from the campus of National Taiwan University (20 males and 20 females; mean age: 22.35 years and 23.25 years, respectfully). All participants had a normal or corrected-to-normal vision and were screened for the presence of psychiatric or neurological disorders. The experimental procedure followed ethical guidelines and is approved by the Institutional Review Board of the National Taiwan University Hospital (202101011RINA).

2.2. Stimuli

Two categories of stimuli were used in the present study, including the 3D impossible objects and their configurational counterparts – the regular objects. The 3D impossible objects are made of the ambiguous cylinders, partly invisible objects, topology-disturbing objects, and deformable objects from Dr. Sugihara's dataset. A total of thirty 3D impossible objects were selected from 54 objects of Sugihara's collections and then were divided into two levels of configurational complexity based on my pilot study (detailed in Appendix A). The regular objects are experimental controls, whose front-view appearances are identical with the 3D impossible objects but also with congruent reflections in the mirror. Hence, there were fifteen 3D impossible objects and fifteen regular objects in each of the two levels of configurational complexity (stimuli examples in Figure 1.1).

2.3. Experimental Procedure

As illustrated in *Figure 1.2*, the experimental procedure consisted of two

doi:10.6342/NTU202210143

experimental tasks separated by a 5-min break; the experiment was constructed in Psychopy (Peirce et al., 2019). The procedure was initiated with the peekaboo task, which was used to investigate the matching process between prior prediction and observed sensory data and, importantly, the dynamics of PE signaling. This session took about 40 minutes. After a short break, participants then proceeded to the perceptual inference task, which was used to explore the perceptual inference process on novel objects and also its potential neural correlates. This part was estimated to take 20 minutes. EEG recordings were simultaneously conducted during the two tasks. All participants received 100 New Taiwan dollars (NTD) if they finish setting up the EEG cap. The participants who completed the peekaboo task gained added 350 NTD. The ones who completed the perceptual inference task gained added 150 NTD. The participants who went through all the procedures gained a total of 600 NTD for their participation.

2.3.1. The Peekaboo Task

During the peekaboo task, the participants had to judge whether the presented object's reflection shown in the uncovered mirror was congruent with the participant's imagined reflection of the introduced object. The structure of an exemplar trial is illustrated in *Figure 1.3*. At the beginning of each trial, a pair of at signs was presented on the center of the screen to inform the start of trial to the participants and also to remind them not to blink afterward. The task was self-paced so that the participants could take a rest before each trial started, wherefore the trial start display stayed on the screen until the participants press the spacebar on the keyboard. The trial started with the 1000ms fixation to instruct the participants to fixate on the center of the screen. A

doi:10.6342/NTU202210143

video display of an object with a covered mirror behind it was then be presented to the participants. The participants were told to imagine the reflection of the object in the mirror. The mirror was uncovered after 3000ms, and the uncovered process (500ms) was shown. Both the object and its reflection in the mirror were presented for another 3000ms. Following this video display of the object, the question page was shown. Participants were instructed to press the “f” key for a congruent appearance (the object’s reflection in the mirror was same as which participant had imagined) or the “j” key for an incongruent appearance (the object’s reflection in the mirror was different from which participant had imagined).

Response time (RT) and accuracy (ACC) of the judgment were recorded and analyzed. The accuracy of the judgment represented if the participant correctly answered the congruence of the objects and their reflection in the mirror. For the possible objects, participants should press “f” to indicate the congruent appearance in the mirror, and vice versa for the impossible objects. The participants whose accuracy of the task did not reach 90% would be excluded from the following EEG analysis. Each of the thirty 3D impossible objects and thirty regular objects were repeated three times, resulting in a total of 180 trials in the peekaboo task. The presented order was pseudo-randomly assigned: 60 objects for a round, the objects were randomly assigned in each round, and there were three rounds in total.

2.3.2. The Perceptual Inference Task

During the perceptual inference task, the participants were shown the actual configuration of the 3D impossible objects, and they were asked to figure out why these objects have dual appearances. The structure of an exemplar trial is illustrated in *Figure 1.4*. Again, a trial start sign was presented at the beginning of each trial to make the task

doi:10.6342/NTU202210143

self-paced by the participants. After a 1000ms fixation, a 3D impossible object on the center of screen presented steady for 1500ms, which showed the one side of the object. Then the object rotated 180° in 2000ms, and it showed the other side of the same object for 1500ms. After that, the object rotated for 180° in 2000ms, back to the same side as introduced for another 1500ms. Finally, the object rotated 360° in 4000ms. The question page was shown after the video display of the object. Participants were instructed to press “f” to indicate if they think the configuration of the object was easy to understand, to press “j” if they think the object’s configuration was too complicated, or to press “spacebar” if they consider it was of the medium complexity. Subjective classification of the configuration complexity of objects was recorded and analyzed. The configuration score were recorded as 2 points if the participant assign the object as the hard/complicated object, recorded as 1 point if they think the object is of the medium complexity, and recorded as 0 when they think the object’s configuration is simple and easy to understand. Each of the thirty 3D impossible objects along with its counterpart was presented one time in a random order, resulting in a total of 60 trials in the perceptual inference task.

2.4. EEG Acquisition and Data Analysis

EEG was recorded using a SynAmps II amplifier (Neuro- Scan, El Paso, TX) from 32 scalp locations according to the 10-20 system. In this protocol, the ground was placed above the forehead, and an electrode A1, left mastoid, served as the online reference. The horizontal and vertical electrooculograms (EOGs) were recorded from the electrodes placed at the outer canthi of both eyes and on the infraorbital and supraorbital regions of the left eye place in line with the pupil. The impedance of all channels were maintained below 5 kΩ. The EEG and EOG signals were sampled at a

doi:10.6342/NTU202210143

rate of 1 kHz with an online band-pass filter of DC-200 Hz. The recorded data were underwent offline re-referenced to the average, and then subjected to an eyeblink artifact correction procedure (Gratton, Coles, & Donchin, 1983) (for the peekaboo task) or Independent Component Analysis (ICA) approach (Makeig, Bell, Jung, & Sejnowski, 1996) (for the perceptual inference task). The peekaboo task was subjected to an eyeblink artifact correction procedure due to the task designed to show the mirror uncovering process, removing the eyeblink trials could make sure the data free from artifacts. On the other hand, the perceptual inference task was undergone the ICA because of the limited number of trials (60 trials for each participant), it is not able to discard too many trials in this task. Data analysis were performed with Brainstorm (Tadel, Baillet, Mosher, Pantazis, & Leahy, 2011) and the EEGLAB toolbox (Delorme & Makeig, 2004) in MATLAB (The Mathworks, Inc., Natick, MA, USA).

To extract the ERP and ERSP in the peekaboo task, we first low-pass filtered the corrected continuous data with a 40 Hz cutoff, and then segmented it into epochs of -200 to 1000ms following the onset of the display of object with uncovered mirror. Baseline corrections were applied to the epoched data with respect to the mean activity of the pre-stimulus window. The epochs subsequently underwent an artifact rejection procedure in which the epochs that contained activities that exceeded $\pm 50\ \mu V$ were excluded from further analysis. The ERP for regular and 3D impossible objects with two levels of configurational complexity are then obtained by averaging all artifact-free epochs for each condition. The whole 0-1000ms epochs were sliced into 10 segments, and the mean activity within each 100ms was used for the statistical analysis.

To explore the dynamic neural network engaging in the perceptual inference process, the ERP, as well as MVPA were performed from corrected continuous data

doi:10.6342/NTU202210143

following the presentation of object rotation in the second session of the experiment. The data were sliced into segments of different display phases: object rotation1, object stop1, object rotation2, object stop2, object rotation3. Baseline correction and artifact rejection were then applied to the epoched data before the subsequent analysis. MVPA was carried out using the Support Vector Machines (SVM), a well-used machine learning tool for both classification and regression problems (Gunn, 1998), with a 30 Hz low-pass cutoff, 100 permutations, and 5 k-folds. The decoding procedure included whole brain electrodes, and was separated conducted through each phase. The purpose of MVPA used in here was in order to find out the critical phase of inference process through a broad scanning, and thus the statistical analysis of it was not applied in this study. As for the statistical analysis of ERPs, the mean activity of the time segments which were chosen from visually reviewing the ERP waveforms were used.

2.5. Statistical Analyses

In the present study, both behavioral (i.e., RT & ACC) and electrophysiological (i.e., ERP, ERSP) were used as measures for evaluating participants' perceptual inference on 3D impossible objects. Statistical analyses were performed using RStudio (RStudio, Inc., Boston, MA, USA). Repeated measures analysis of variance (RM-ANOVA) was used to assess these measures under the different combinations of experimental conditions. Post-hoc analyses were performed using Tukey's test when the F-value indicated a significant difference. A Greenhouse-Geisser adjustment of degrees of freedom, as well as a Bonferroni correction, were applied when necessary.

doi:10.6342/NTU202210143

Chapter 3. Results

Among the forty participants, two of them did not finish session 1 and the subsequent session 2. Two of the participants did not meet the requirement of 90% accuracy in session 1 performance. Four participants' data for session 1 and two for session 2 were excluded because of recording issue. Excluded the above participants data, remained 32 participants' data for session 1 (16 males, mean age: 23.31 years; 16 females, mean age: 22.63 years), and 36 participants' data for session 2 (19 Male 23.05 years; 17 females: 22.18 years) were adopted in this study.

3.1. Peekaboo Task

3.1.1. Task Performance

The accuracy, correctly answered the congruency of the mirror display of objects, of the participants who finished the whole session was 95.45% (impossible objects: 95.47%, easy configuration was 94.97% and hard configuration was 95.96%; normal objects: 95.41%; see Table 1). The mean response time of all participant across objects was 0.770 seconds (impossible objects: 0.762 seconds, easy configuration was 0.760 seconds and hard configuration was 0.765 seconds; normal objects: 0.784 seconds; see Table 1). There was no difference between two kinds of objects and both configuration levels according to statistical analysis either by accuracy and reaction time (accuracy: F (2, 74) = 0.564, p = .571; reaction time: F (2, 74) = 1.030, p = .362; Table B1 and B2 in Appendix B).

3.1.2. ERP

Raw EEG recordings were processed into ERP components, the average epochs of

doi:10.6342/NTU202210143

objects' mirror image displayed. The waveforms at three midline channels (i.e., Fz, Cz, and Pz) were shown in the *Figures 2* (six midline sites results were shown in Appendix B, Figure B1). Ten mean activities of 100 ms data (0-1000 ms) were evaluated to verify the congruent and incongruent mirror images elicited components. A two-way RM-ANOVA (channel and object category) of the ERP segments of 200-300 ms and 800-900 ms after mirror uncovered revealed a significant main effect on channels (200-300 ms: F (5, 155) = 9.051, p = 1.44 e^{-07} < .001; 800-900 ms: F (5, 155) = 15.923, p = 1.21 e^{-12} < .001), a significant main effect on object category (200-300 ms: F (1, 31) = 4.469, p = 0.043 < .05; 800-900 ms: F (1, 31) = 4.680, p = 0.038 < .05), and a significant interaction between channel and object category (200-300 ms: F (5, 155) = 2.968, p = 0.014 < .05; 800-900 ms: F (5, 155) = 3.503, p = 0.005 < .01) (RM-ANOVA table were in Appendix B, Table B3 and B4). Post-hoc analyses indicated when the incongruent mirror images presented, the ERP of 200-300 ms after mirror uncovered was significant more negative across frontal-central sites (left of Figure 3); in contrast, the segment of 800-900 ms showed a positive wave, and was stronger at the frontal sites (right of Figure 3).

3.1.3. ERSP

In order to ensure the components that represent the prediction error signals in this peekaboo perceptual scenario, the time-frequency analysis was carefully inspected. The ERSP heat-maps of three midline sites (i.e., Fz, Cz, and Pz) were showed in *Figure* 4 (other three midline channels' figures were included in Appendix B, Figure B2). The time segment of 400-500 ms after mirror uncovered had a significant effect on object category in low frequency band, including delta band (i.e., 1-3 Hz) (F (1, 31) = 5.152, p

doi:10.6342/NTU202210143

= 0.019 < .05), theta band (i.e., 4-7 Hz) (F (1, 31) = 12.147, p = 0.001 < .01), and also alpha band (i.e., 8-12 Hz) (F (1, 31) = 12.217, p = 0.001 < .01). While the impossible objects scene showed stronger delta and alpha frequency at frontal-central sites, the impossible objects scene was significantly higher across central-parietal sites in the theta band (Figure 5). As depicted in *Figure 6,* beta frequency band (i.e., 13-30 Hz) showed a stronger effect in two time segments after impossible objects' mirror image presented, and the effect on both segments were frontal-central distributed (the above ANOVA result tables are presented in the Appendix B, Table B5-9).

3.2. Perceptual Inference Task.

3.2.1. Behavioral Results

As the data presented in *Table 2*, the subjective configuration score matched the previously assigned objects' configuration level. The hard impossible objects' and easy impossible objects' configuration score were significantly higher than the normal objects' score (F (2, 74) = 345.85, p < 2.2e-16; Table B10 in Appendix B). Two levels of the impossible objects were also significantly different from each other, the hard impossible objects' configuration score was significantly higher than the easy ones' *Figure 7 (left)*. Similarly, the time participants took to classify the objects were also longer for the impossible objects (F (2, 74) = 16.637, p = 1.08e^{-06} < .001; Table B11 in Appendix B), though the reaction time was not different between two configuration levels *Figure 7 (right)*.

3.2.2. MVPA

Using advance multivariate pattern analysis, whole brain data were included to

doi:10.6342/NTU202210143

decode the perceptual process of inferring our unique objects. Different phases of the perceptual inference were separated from the continuous EEG recordings and were processed into individual epochs. MVPA results were showed in *Table 3*, the decoding accuracy of each phase was averaged across the time. As depicted, the decoding accuracy results between the two kinds of configuration levels were at chance level in nearly every phase except for two rotation phases (69.68% for the first rotation and 55.12% for the second rotation; decoding figures in Appendix B, Figure B3 and B4). The decoding accuracy between the impossible objects and the normal objects was higher in the hard configuration level condition during the first and the second stop (easy level: 64.22% and hard level: 73.45% during the first stop phase; easy level: 54.89 % and hard level: 62.74 % during the second stop phase) and the third rotation phase (easy level: 52.55% and hard level: 58.56%). Intriguingly, during the first rotation, the decoding accuracy was slightly higher in the easy configuration level condition (easy level: 71.47% and hard level: 67.90%).

3.2.3. ERP

Though the impossible objects' configuration level difference can be verified through decoding accuracy results between the two kinds of configuration levels during two rotation phases, the underlying neural dynamics remain unknown. To focus on the neuronal process of inferring the objects, the two rotation phases were specialized examined. The three midline channels' first rotation and the second rotation ERPs were shown in the *Figures 8 & 9* (midline sites results were shown in Appendix B, Figure B5 and B6). According to the ERP waveforms, two time segments were extracted for the further inspection: 200-400 ms and 500-800 ms.

doi:10.6342/NTU202210143

RM-ANOVA results of the ERP segments of 200-400 ms in the first rotation phase revealed significant main effects on both channels and object category (channels: F (5, 175) = 4.983, p = .0003 < .001; object category: F (2, 70) = 8.066, p = .0007 < .001), and the interaction was nearly significant (F (10, 350) = 1.640, p = .094) (ANOVA table in Appendix B, Table B12). In this time segment, hard impossible objects were less positive than both easy impossible objects and the normal objects at central-parietal sites (left of Figure 10). The 500-800 ms segment in the first rotation was instead more positive in the impossible objects condition at central-parietal sites, and that the easy impossible objects were the ones who elicited the even stronger effect (channels: F (5, 175) = 12.720, p = $1.50e^{-10}$ < .001; object category: F (2, 70) = 36.065, p = $1.72e^{-11}$ < .001; interaction: F (10, 350) = 18.198, p = < $2.2e^{-16}$) (right of Figure 10) (ANOVA table in Appendix B, Table B13).

The second rotation demonstrated a fairly different result. The 200-400 ms segment also exhibited significant main effects on both channels and object category, and the interaction was also significant (channels: F (5, 175) = 4.317, p = .00099 < .001; object category: F (2, 70) = 5.853, p = .00446 < .01; interaction: F (10, 350) = 5.108, p = $5.67e^{-07}$ < .001) (ANOVA table in Appendix B, Table B14). By contrast to the first rotation, the effect of fewer positive waves were presented on the frontal-central sites, and the easy impossible objects condition was the most significant (left of Figure 11). The results of the 500-800 ms segment analysis showed significant main effect on channel but not object category, and there was still significant interaction effect (channels: F (5, 175) = 6.953, p = $6.01e^{-06}$ < .001; object category: F (2, 70) = 0.696, p = . 502; interaction: F (10, 350) = 2.632, p = .004 < .01) (ANOVA table in Appendix B, Table B15). The easy impossible objects condition was significantly less positive than

doi:10.6342/NTU202210143

other two conditions at the frontal site (Fz), and the other two conditions were not different from each other (right of Figure 11). (Others phases' ERP waveforms at midline channels were fully presented in Appendix B, Figure B7-9).

doi:10.6342/NTU202210143

Chapter 4. Discussion and Conclusion

Through the structured investigation in this study, authentic 3D impossible objects created by Dr. Sugihara were utilized as experiments stimuli for exploring the illusory perceptual inference. This study was separate into two parts: the first session confirms the unexpected sensory inputs can be verified by the ERP components and ERSP results, and that the prediction error signals might exist in this illusory perceptual scene. The second session further decoded the neural dynamic while perceiving the unpredictable impossible objects, which provides an intriguing picture of this perceptual inference process.

4.1. Overlaid ERP Components and Distinct Oscillation Pattern in the Peekaboo Task

In session 1, the peekaboo task, most of the participants are able to form the correct prediction of presented objects, and are able to recognize the anomalous mirror reflection. ERP waveforms at frontal-central sites of this perceptual feedback were occupied by a larger positive potential elicited probably 200-300 ms after the mirror image presented (Figure 2). Noted that there was a large positive wave at parietal site after 300 ms as well for the impossible objects, though the statistical result showed it was not significant. These kinds of late positive potential (LPP) can be recognized as related to affective arousal (Cuthbert, Schupp, Bradley, Birbaumer, & Lang, 2000; Keil et al., 2002; Hajcak, MacNamara, & Olvet, 2010). The other related component is P300 (Picton, 1992), which has been stated to reflect higher-level processes such as attentive selection or error detection (Donchin, Gratton, Dupree, Coles, 1988; Falkenstein, Koshlykova, Kiroj, Hoormann, Hohnsbein, 1995). These large positive potentials might

doi:10.6342/NTU202210143

overlay the possible prediction error signals, which might in turn block the signal appearance. The following ERSP analysis could provide an extra domain of information to inspect the brainwave of this process.

One of the well-known frequency bands that was argued related to FRN or ERN is frontal medial theta band (FMT) oscillations (Kalfaoglu, Stafford, & Milne, 2017). The FMT oscillations are showed related to higher level cognitive functions such as conflict and novelty detection (Cavanagh & Frank, 2014; van Driel, Swart, Egner, Ridderinkhof, & Cohen, 2015). In the present study, the incongruent mirror image condition was related to increased theta band (Figure 5). Unlike FMT, the increased theta band effect in this study was presented in central-parietal sites. On the other hand, the increased alpha band during unexpected image sensory inputs was shown at frontal-central sites. Interestingly, the same trend was shown in beta frequency band, and it was also presented at frontal-central sites (Figure 6). These results were slightly different from the previous study of that the theta band activity was frontal distributed, while the alpha/beta oscillation was more parietal distributed (Savoie, Thénault, Whittingstall, & Bernier, 2018). Given that the scenery and the task design of the experiment are so different to be compared, the present study might have demonstrated its unique frequency band oscillation pattern.

Despite the discussion above, which focus in the time within 200-500 ms after expected or unexpected sensory inputs, there is also a late increasing activity in beta frequency band at frontal sites. This results match some of the studies, which have shown the alpha/beta band may related to emotional arousal and that the long-lasting time range of LPP (Du, & Lee, 2014; Du, Lee, & Wei, 2017; Schupp et al., 2000).

Integrated the results of both ERP and ERSP of the peekaboo task, the present

doi:10.6342/NTU202210143

study showed a clearly different patterns from the formerly studies. Since the present study adopted the extreme novel stimuli, the experimental design was also an original approach, the distinctive results were predictable. The 3D impossible objects spiced up the predictable world, endowed it with some of fathomless. The understanding of these objects' configuration thus become a worth-noticing process. The second session, the perceptual inference task, was set to take the lead in investigating how these objects were perceived and inferred, which could further implicate the process of perceptual inference of illusory perception.

4.2. Successfully MVPA Decoding and the Role of the Frontal-parietal Network in the Perceptual Inference Task

The result of subjective classification in the perceptual inference task was consistent with prior assigned configuration level. This indicated that the participants could subjectively discriminate the objects as normal objects, easy configuration impossible objects, or hard configuration impossible objects. The subsequent analysis thus could be interpretable based on this categorization. The MVPA was conducted to identify the difference between normal objects and impossible objects or even between two configuration levels objects. The MVPA includes the whole brain data; hence, the results could be seen as the differentiation when the brain were involving watching and inferring the objects of the different categories. As the data showed in *Table 3*, the higher decoding accuracy between normal and impossible objects were presented during the first rotation and the first stop. The result might indicate the surprising of watching the unpredictable configuration, and the realizing of how the impossible becoming possible. Two impossible levels were successfully set apart during the first two rotation

doi:10.6342/NTU202210143

phases, demonstrated the process of inferring the objects' appearances can be differentiated according to the configuration levels. Especially at the phase of the first rotation, the decoding accuracy between two levels was closed to 70%. Noticeably, this high decoding accuracy during first rotation was along with the higher decoding accuracy in easy level objects.

The findings above were a relatively macroscopic view, since the MVPA decoded thoroughly brain data. The ERPs analysis may provide a relatively detailed results by illustrating the neural dynamic at channels level. The analysis of two rotation phase were inspected closely due to their crucial roles in perceptual inference in this task. Two time segments, 200-400 ms and 500-800 ms, were extracted and compared from the two phases. During the first rotation, the central-parietal activity popped out in either of the time segments. The inference of easy level impossible objects in this phase (500-800 ms) elicit the significantly more positive potential, which might be the crux of the highest MVPA results. By contrast, the second rotation showed a stronger negative potential in 200-400 ms segment, which was frontal-central distributed. These discovered strikingly in line with several perceptual decision making research, especially in the context of multi-stable perception, which emphasizing the frontal-parietal network. Posterior regions were in association with the process of perceptual interpretation and reorganizations, and the anterior regions were involved in metacognitive evaluation of perceptual decisions (Frassle, Sommer, Jansen, Naber, Einhäuser, 2014; Leopold, Logothetis, 1999; Rahnev, Nee, Riddle, Larson, D'Esposito, 2016). The inferior frontal cortex (IFC) in between could act as an essential role in perceptual transitions, and it might be the key structure that could response to the prediction errors arising in the sensory cortex (Brascamp, Sterzer, Blake, & Knapen,

doi:10.6342/NTU202210143

2018; Friston, Harrison, Harrison, Penny, 2003).

The frontal-parietal network might suit the present study of perceptual inference task, though the stronger effects of the easy level impossible objects were still out of the line. One plausible explanation might be that the easy level impossible objects are easier to figure out their configuration, and hence elicited the larger potential. The other rationale could be that the easy level impossible objects might have a relative continuous configuration than the hard level objects, and thus yielded this brainwave difference. The limitation of the task design might cause the interpretation difficulty of the results as well. The instruction of the test might lead the participants to just classify the objects instead of trying to understanding their structure, and this may cause the perceptual inference process incomplete when perceiving the hard level objects.

4.3. Limitation and Future Studies

The present study is dedicated to the investigating the neural dynamics underlying the illusory perception. Dr. Sugihara's collections provide a new vision for the further investigation in illusory perception. To make the most of the 3D impossible objects, this study established two unconventional tasks: the first was to confirm the prediction error signaling in such impossible and unexpected scene, and the second was to explore the uncovered perceptual inference of the illusory yet possible perception.

The tasks in this study introduced sensory PE and perceptual inference of illusory perception from a new angle, though the results of the tasks have their limits. The objects' presenting order was pseudo-random in the peekaboo task, but whether the possible or the impossible objects presented first could give rise to a different result. The three rounds of repeated presentation of objects could have varying degrees of

doi:10.6342/NTU202210143

influence of repetition effect, which worth attention in the future analysis. Also, the present study was not adequate to affirm the prediction error indeed arose when viewing the impossible objects and their mirror images.

For the perceptual inference task, the insufficiency of the task design was described in the last chapter (Chapter 3.2.3). There was also some confounding of the task results, such as that it might be possible that the brainwave was actually reporting the configuration difference rather than the inference process. The improvement of the two tasks is needed for a more precise study. The new peekaboo task should definitely integrate predicted process, and should clarify the presenting order effect. The improved perceptual inference should distinguish the inference process from the configuration difference, and should make sure that the participants understand the objects' structure.

Despite the renewal task design, the advanced analysis is still wanted for the more thoroughly inspection, such as source reconstruction, which can further locate the more precise brain section in which associated with the sensory processing. The functional connectivity and graph-based network analysis are both required for assuring the related perceptual inference network.

These additional tasks and analyses may make the results of the study more comprehensive. The present study act as an exploratory step, highlights the neural dynamics underlying illusory perception, shed the light on sensory processing of 3D illusions, and is expected to pave the way for a more detailed exploration of the illusory perception which used to be impossible.

doi:10.6342/NTU202210143

References

Alink, A., Schwiedrzik, C. M., Kohler, A., Singer, W., & Muckli, L. (2010). Stimulus predictability reduces responses in primary visual cortex. *Journal of Neuroscience, 30*(8), 2960-2966.

Amiez, C., Joseph, J. P., & Procyk, E. (2005). Anterior cingulate error-related activity is modulated by predicted reward. *European Journal of Neuroscience, 21*(12), 3447-3452.

Anderson, E. J., Dakin, S. C., & Rees, G. (2009). Monocular signals in human lateral geniculate nucleus reflect the Craik–Cornsweet–O'Brien effect. *Journal of Vision*, *9*(12), 14-14.

Bastos, A. M., Vezoli, J., Bosman, C. A., Schoffelen, J., Oostenveld, R., Dowdall, J. R., Weerd, P. D., Kennedy, H., & Fries, P. (2015). Visual areas exert feedforward and feedback influences through distinct frequency channels. *Neuron, 85*(2), 390-401. https://doi.org/10.1016/j.neuron.2014.12.018

Boksem, M. A., & De Cremer, D. (2010). Fairness concerns predict medial frontal negativity amplitude in ultimatum bargaining. *Social Neuroscience, 5*(1), 118-128.

Brascamp, J., Sterzer, P., Blake, R., & Knapen, T. (2018). Multistable Perception and the Role of the Frontoparietal Cortex in Perceptual Inference. *Annual Review of Psychology, 69*(1), 77-103. https://doi.org/10.1146/annurev-psych-010417-085944

Brydevall, M., Bennett, D., Murawski, C., & Bode, S. (2018). The neural encoding of information prediction errors during non-instrumental information seeking. *Scientific Reports, 8*(1), 6134. https://doi.org/10.1038/s41598-018-24566-x

Cavanagh, J. F., & Frank, M. J. (2014). Frontal theta as a mechanism for cognitive

doi:10.6342/NTU202210143

control. *Trends in Cognitive Sciences, 18*(8), 414-421.

Coren, S. (2012). Sensation and perception. In D. K. Freedheim & I. B. Weiner (Eds.), *Handbook of psychology* (2nd ed.). John Wiley & Sons, Inc..

Cuthbert, B. N., Schupp, H. T., Bradley, M. M., Birbaumer, N., & Lang, P. J. (2000). Brain potentials in affective picture processing: Covariation with autonomic arousal and affective report. *Biological Psychology, 52*(2), 95-111.

Delorme, A., & Makeig, S. (2004). EEGLAB: An open source toolbox for analysis of single-trial EEG dynamics including independent component analysis. *Journal of Neuroscience Methods, 134*(1), 9-21.

Deregowski, J. B., & Bentley A. M. (1987). Seeing the impossible and building the likely. *British Journal of Psychology 78*(1), 91-97.

Donchin, E., Gratton, G., Dupree, D., & Coles, M. (1988). After a rash action: Latency and amplitude of the P300 following fast guesses. In G. C. Galbraith, M. L. Kietzman, & E. Donchin (Eds.), *Neurophysiology and Psychophysiology: Experimental and Clinical Applications* (pp. 173-188). Taylor and Francis. https://doi.org/10.4324/9781003164647-21

Du, R. & Lee, H. J. (2014). Power spectral performance analysis of EEG during emotional auditory experiment. In I. Staff, W. Wan, X. Yu, & F. L. Luo (Eds.), *2014 International Conference on Audio, Language and Image Processing (ICALIP)* (pp. 64-68). IEEE. https://doi.org/10.1109/ICALIP.2014.7009758

Du, R., Lee, H. J., & Wei, R. (2017). Brain emotional oscillatory activity during the different affective picture and sound experience. In I. Staff (Ed.), 20*17 10th International Congress on Image and Signal Processing, BioMedical Engineering and Informatics (CISP-BMEI)* (pp. 1-6). IEEE. https://doi.org/10.1109/CISP-

doi:10.6342/NTU202210143

BMEI.2017.8302298

Duncan, J. (2010). The multiple-demand (MD) system of the primate brain: Mental programs for intelligent behaviour. *Trends in Cognitive Sciences*, *14*(4), 172-179.

Fahrenfort, J. J., Grubert, A., Olivers, C. N. L., & Eimer, M. (2017). Multivariate EEG analyses support high-resolution tracking of feature-based attentional selection. *Scientific Reports, 7*(1), 1-15. doi: 10.1038/s41598-017-01911-0

Falkenstein, M., Koshlykova. N. A., Kiroj, V. N., Hoormann, J., & Hohnsbein, J. (1995). Late ERP components in visual and auditory Go/Nogo tasks. *Electroencephalography and Clinical Neurophysiology. 96*(1), 36-43.

Frassle, S., Sommer, J., Jansen, A., Naber, M., & Einhäuser, W. (2014). Binocular rivalry: Frontal activity relates to introspection and action but not to perception. *Journal of Neuroscience, 34*(5), 1738-1747.

Friedman, D., & Cycowicz, Y. M. (2006). Repetition priming of possible and impossible objects from ERP and behavioral perspectives. *Psychophysiology*, *43*(6), 569-578. https://doi.org/10.1111/j.1469-8986.2006.00466.x

Friston, K. (2005). A theory of cortical responses. *Philosophical Transactions of the Royal Society B: Biological Sciences*, *360*(1456), 815-836.

Friston, K. (2010). The free-energy principle: A unified brain theory?. *Nature Reviews Neuroscience*, *11*(2), 127-138.

Friston, K., Kilner, J., & Harrison, L. (2006). A free energy principle for the brain. *Journal of Physiology-Paris*, *100*(1-3), 70-87.

Friston, K. J., Harrison, L. M., Harrison, L., & Penny, W. (2003). Dynamic causal modelling. *NeuroImage. 19*(4), 1273-1302.

Freud, E., Ganel, T., & Avidan, G. (2015). Impossible expectations: fMRI adaptation in

doi:10.6342/NTU202210143

the lateral occipital complex (LOC) is modulated by the statistical regularities of 3D structural information. *NeuroImage, 122*, 188-194. https://doi.org/10.1016/j.neuroimage.2015.07.085

Gehring, W. J., Goss, B., Coles, M. G. H., Meyer, D. E., & Donchin, E. (1993). A neural system for error detection and compensation. *Psychologcial Science, 4*(6), 385-390.

Gratton, G., Coles, M. G., & Donchin, E. (1983). A new method for off-line removal of ocular artifact. *Electroencephalography and Clinical Neurophysiology*, *55*(4), 468-484.

Gunn, S. R. (1998). Support vector machines for classification and regression. *ISIS Technical Report, 14*(1), 5-16.

Hajcak, G., MacNamara, A., & Olvet, D. M. (2010). Event-related potentials, emotion, and emotion regulation: An integrative review. *Developmental Neuropsychology, 35*(2), 129-155.

Kalfaoglu, C., Stafford, T., & Milne, E. (2017) Frontal theta band oscillations predict error correction and posterror slowing in typing. *Journal of Experimental Psychology: Human Perception and Performance, 44*(1), 69. ISSN 0096-1523 https://doi.org/10.1037/xhp0000417

Keil, A., Bradley, M. A., Hauk, O., Rockstroh, B., Elbert, T., & Lang, P. J. (2002). Large-scale neural correlates of affective picture processing. *Psychophysiology, 39*(5), 641-649.

King, J. R., & Dehaene, S. (2014). Characterizing the dynamics of mental representations: The temporal generalization method. *Trends in Cognitive Sciences, 18*(4), 203-210. https://doi.org/10.1016/j.tics.2014.01.002

Leopold, D. A., & Logothetis, N. K. (1999). Multistable phenomena: changing views in

doi:10.6342/NTU202210143

perception. *Trends in Cognitive Sciences, 3*(7), 254-264.

Luck, S. J. (2014). *An introduction to the event-related potential technique*. Cambridge, MA: MIT Press.

Luu, P., & Tucker, D. M. (2001). Regulating action: Alternating activation of midline frontal and motor cortical networks. *Clinical Neurophysiology, 112*(7), 1295-1306.

Makeig, S. (1993). Auditory event-related dynamics of the EEG spectrum and effects of exposure to tones. *Electroencephalography and Clinical Neurophysiology 86*(4), 283-293.

Makeig, S., Bell, A. J., Jung, T. P., & Sejnowski, T. J. (1996). Independent component analysis of electroencephalographic data. In D. Touretzky, M. Mozer, M. Hasselmo (Eds.), *Advances in neural information processing systems*, *8*, 145-151.

Mars, R. B., Coles, M. G. H., Grol, M. J., Holroyd, C. B., Nieuwenhuis, S., Hulstijn, W., & Toni, I. (2005). Neural dynamics of error processing in medial frontal cortex. *NeuroImage, 28*(4), 1007-1013.

Miltner, W. H. R., Braun, C. H., & Coles, M. G. H. (1997). Event-related brain potentials following incorrect feedback in a time-estimation task: Evidence for a "generic" neural system for error detection. *Journal of Cognitive Neuroscience, 9*(6), 788-798.

Walsh, M. M., & Anderson, J. R. (2011). Modulation of the feedback-related negativity by instruction and experience. *Proceedings of the National Academy of Sciences*, *108*(47), 19048-19053.

Peirce, J., Gray, J.R., Simpson, S., MacAskill, M., Höchenberger, R., Sogo, H., Kastman, E., & Lindeløv, J. K. (2019). PsychoPy2: Experiments in behavior made easy. *Behavior Research Methods, 51*(1), 195-203. https://doi.org/10.3758/s13428-

doi:10.6342/NTU202210143

018-01193-y

Peters, B. O., Pfurtscheller, G., & Flyvbjerg, H. (1998). Mining multi-channel EEG for its information content: An ANN-based method for a brain-computer interface. *Neural Network, 11*(7-8), 1429-1433. https://doi.org/10.1016/S0893-6080(98)00060-4

Picton, T.W. (1992). The P300 wave of the human event-related potential. *Journal of Clinical Neurophysiology, 9*(4), 456-479.

Purves, D., Shimpi, A., & Lotto, R. B. (1999). An empirical explanation of the Cornsweet effect. *Journal of Neuroscience*, *19*(19), 8542-8551.

Rahnev, D., Nee, D. E., Riddle, J., Larson, A. S., & D'Esposito, M. (2016). Causal evidence for frontal cortex organization for perceptual decision making. *Proceedings of the National Academy of Sciences, 113*(21), 6059-6064.

Savoie, F. A., Thénault, F., Whittingstall, K., & Bernier, P. M. (2018). Visuomotor prediction errors modulate EEG activity over parietal cortex. *Scientific Reports, 8*(1), 1-16. https://doi.org/10.1038/s41598-018-30609-0

Schupp, H. T., Cuthbert, B. N., Bradley, M. M., Cacioppo, J. T., Ito, T., & Lang, P. J. (2000). Affective picture processing: the late positive potential is modulated by motivational relevance. *Psychophysiology, 37*(2). 257-261. https://doi.org/10.1111/1469-8986.3720257

Shigemura, J., Yoshino, A., Kobayashi, Y., Takahashi, Y., & Nomura, S. (2004). Spatiotemporal differences between cognitive processes of spatially possible and impossible objects: A high-density electrical mapping study. *Cognitive Brain Research, 18*(3), 301-305. https://doi.org/10.1016/j.cogbrainres.2003.10.017

Stefanics, G., Kremlácek, J., & Czigler, I. (2014). Visual mismatch negativity: a

doi:10.6342/NTU202210143

predictive coding view. *Front Human Neuroscience, 8*, 666. https://doi.org/10.3389/fnhum.2014.00666

Sugihara, K. (2015). Ambiguous cylinders: A new class of impossible objects. *Computer Aided Drafting, Design and Manufacturing 25*(4), 19-25.

Sugihara, K. (2016a). Anomalous mirror symmetry generated by optical illusion. *Symmetry*, *8*(4), 21.

Sugihara, K. (2016b). A new type of impossible objects that become partly invisible in a mirror. *Japan Journal of Industrial and Applied Mathematics*, *33*(3), 525-535.

Sugihara, K. (2018a). Topology-disturbing objects: a new class of 3D optical illusion. *Journal of Mathematics and the Arts*, *12*(1), 2-18.

Sugihara, K. (2018b). Evolution of Impossible Objects. In *9th International Conference on Fun with Algorithms (FUN 2018)*. Schloss Dagstuhl-Leibniz-Zentrum fuer Informatik.

Sur, S., & Sinha, V. K. (2009). Event-related potential: An overview. *Industrial Psychiatry Journal*, *18*(1), 70-73. https://doi.org/10.4103/0972-6748.57865

Symonds, R. M., Lee, W. W., Kohn, A., Schwartz, O., Witkowski, S., & Sussman, E. S. (2017). Distinguishing neural adaptation and predictive coding hypotheses in auditory change detection. *Brain Topography, 30*(1), 136-148.

Tadel, F., Baillet, S., Mosher, J. C., Pantazis, D., & Leahy, R. M. (2011). Brainstorm: A user-friendly application for MEG/EEG analysis. *Computational intelligence and neuroscience, 2011, 879716*. https://doi.org/10.1155/2011/879716

van Driel, J., Swart, J., Egner, T., Ridderinkhof, K., & Cohen, M. (2015). (No) time for control: Frontal theta dynamics reveal the cost of temporally guided conflict anticipation. *Cognitive, Affective, and Behavioral Neuroscience, 15*(4), 787-807.

doi:10.6342/NTU202210143

https://doi.org/10.3758/s13415-015-0367-2

Wacongne, C., Labyt, E., van Wassenhove, V., Bekinschtein, T., Naccache, L., & Dehaene, S. (2011). Evidence for a hierarchy of predictions and prediction errors in human cortex. *Proceedings of the National Academy of Sciences, 108*(51), 20754-20759.

Wu, X., Li, W., Zhang, M., & Qiu, J. (2012). The neural basis of impossible figures: Evidence from an fMRI study of the two-pronged trident. *Neuroscience Letters, 508*(1), 17-21. https://doi.org/10.1016/j.neulet.2011.11.064

Young, A., & Deregowski, J. (1981). Learning to see the impossible. *Perception, 10*(1), 91-105.

doi:10.6342/NTU202210143

Tables

Table 1

The Behavioral Data of the Peekaboo Task

Configuration Level	Accuracy		Response Time	
	M (%)	*SD*	*M* (s)	*SD*
Normal Objects	95.41	0.0031	0.784	0.083
Impossible Objects	95.47		0.762	
Easy Level	94.97	0.0035	0.760	0.062
Hard Level	95.96	0.0027	0.765	0.072

Table 2

The Behavioral Data of the Perceptual Inference Task

Objects	Subjective Configuration Score		Response Time	
	M	*SD*	*M* (s)	*SD*
Normal Objects	0.063	0.012	0.731	0.078
Impossible Objects	1.270		0.983	
Easy Level	1.078	0.214	0.971	0.123
Hard Level	1.461	0.149	0.995	0.181

Table 3

MVPA Results of the Perceptual Inference Task

Phase	Decoding Accuracy (%)		
	Easy *Norm. vs. Imp.*	*Hard* *Norm. vs. Imp.*	*Imp.* *Easy vs. Hard*
Fist Rotation	71.47	67.90	69.68
Fist Stop	64.22	73.45	46.21
Second Rotation	53.48	53.92	55.12
Second Stop	54.89	62.74	49.59
Third Rotation	52.55	58.56	49.93

doi:10.6342/NTU202210143

doi:10.6342/NTU202210143

Figures

Figure 1.1
Configurational Complexity (left: easy configuration level object; right: hard configuration level object).

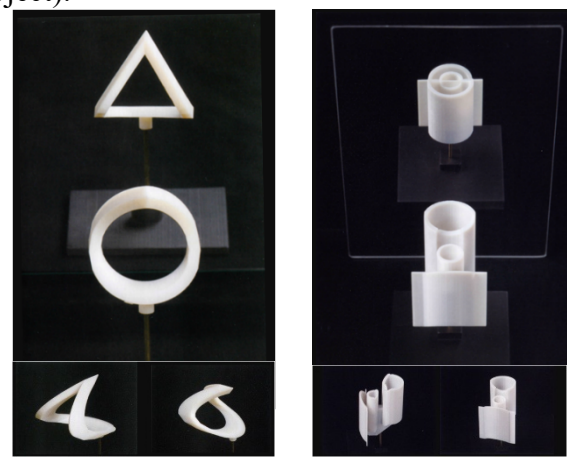

Figure 1.2
General Procedure, including EEG setting, the whole experiment took about 90 to 120 minutes.

Figure 1.3
The Peekaboo Task

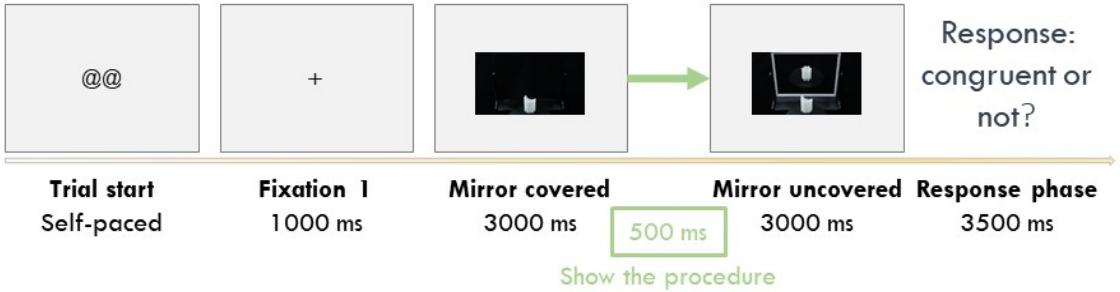

Figure 1.4
The Perceptual Inference Task

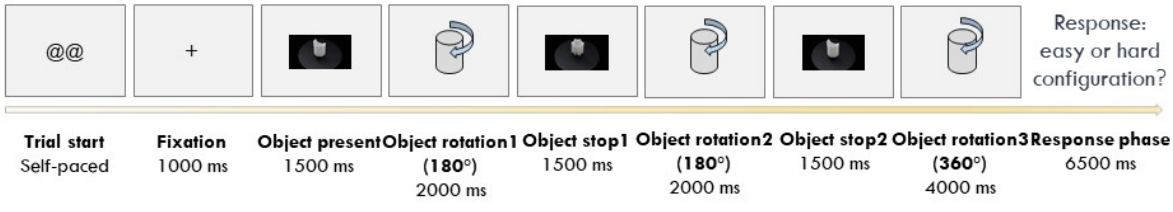

doi:10.6342/NTU202210143

Figure 2

The Peekaboo Task ERP Waveforms at Fz, Cz, and Pz.

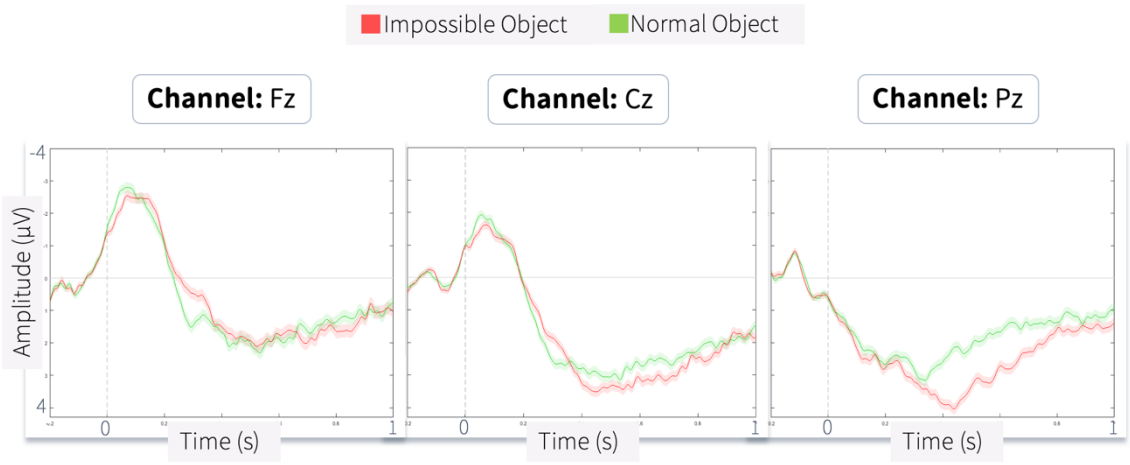

Figure 3

The Peekaboo Task ERP Post-hoc Results of 200-300 ms and 800-900 ms at Fz, Cz, and Pz.

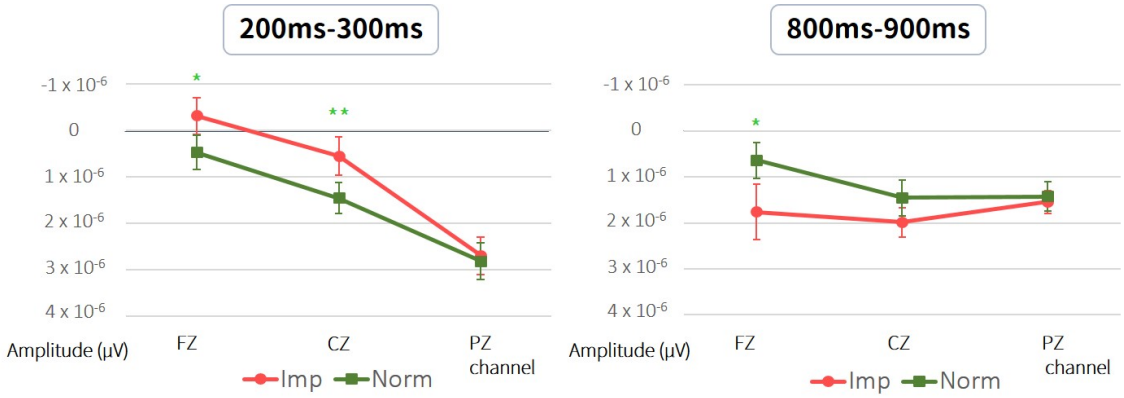

* $p < .05$. ** $p < .01$.

doi:10.6342/NTU202210143

Figure 4.1

The Peekaboo Task ERSP Heat Map at Fz.

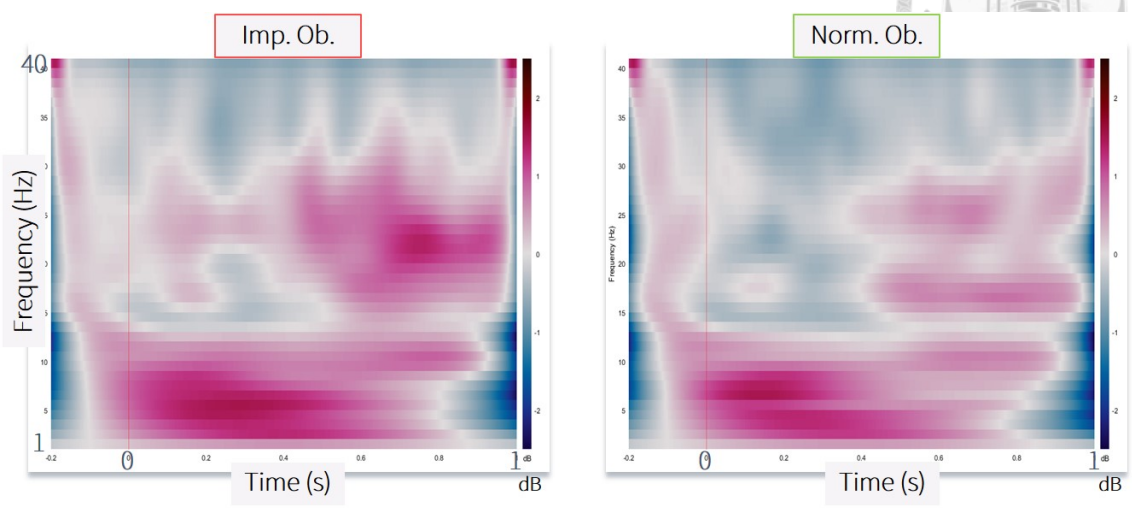

Figure 4.2

The Peekaboo Task ERSP Heat Map at Cz.

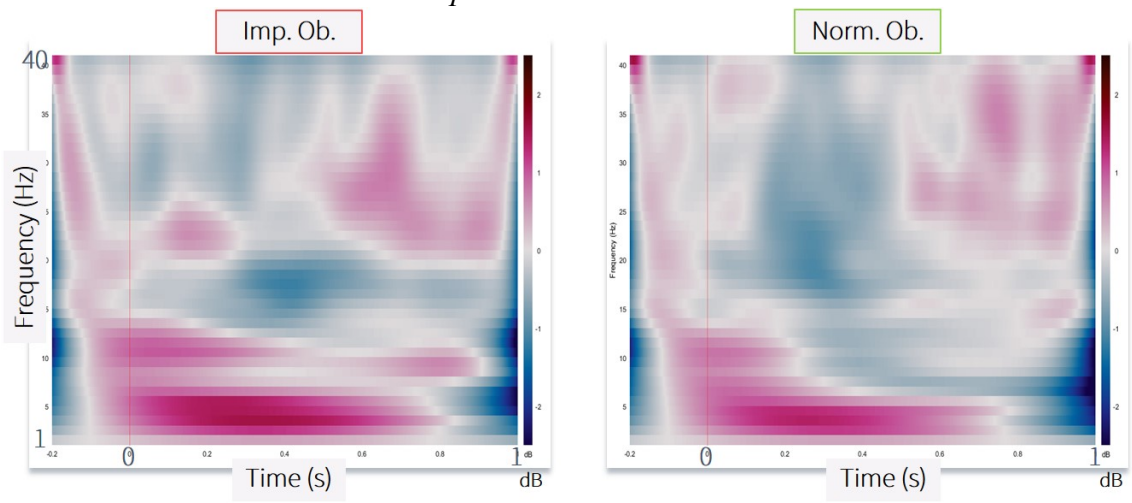

Figure 4.3

The Peekaboo Task ERSP Heat Map at Pz.

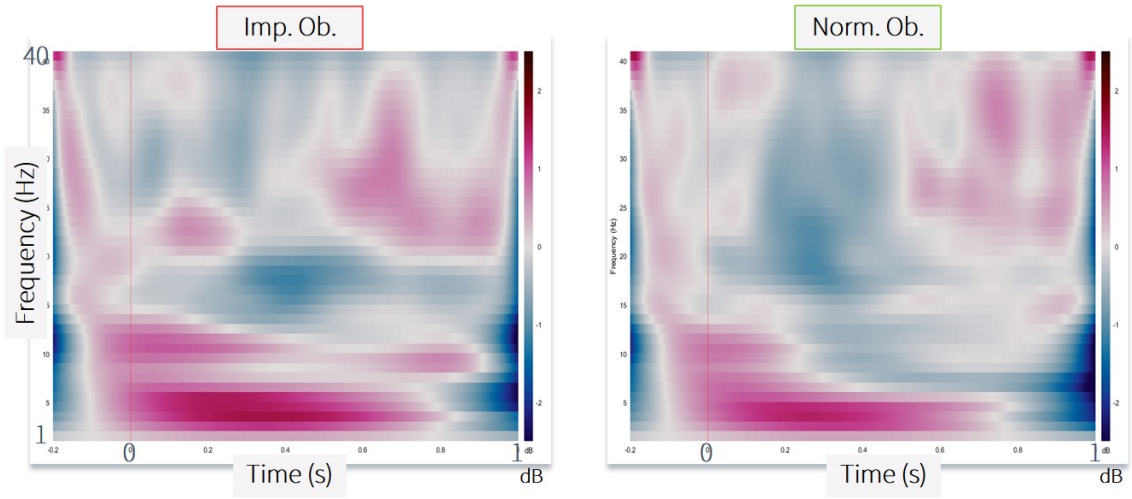

doi:10.6342/NTU202210143

Figure 5

The Peekaboo Task ERSP Post-hoc Results of 400-500 ms of Delta, Theta, and Alpha Band at Fz, Cz, and Pz.

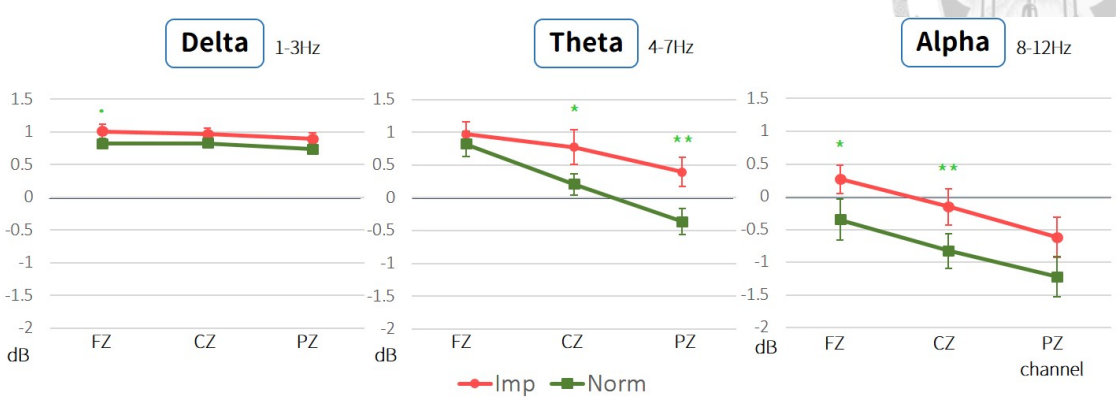

* $p < .05$. ** $p < .01$.

Figure 6

The Peekaboo Task ERSP Post-hoc Results of 200-300 ms and 700-800 ms of Beta Band at Fz, Cz, and Pz.

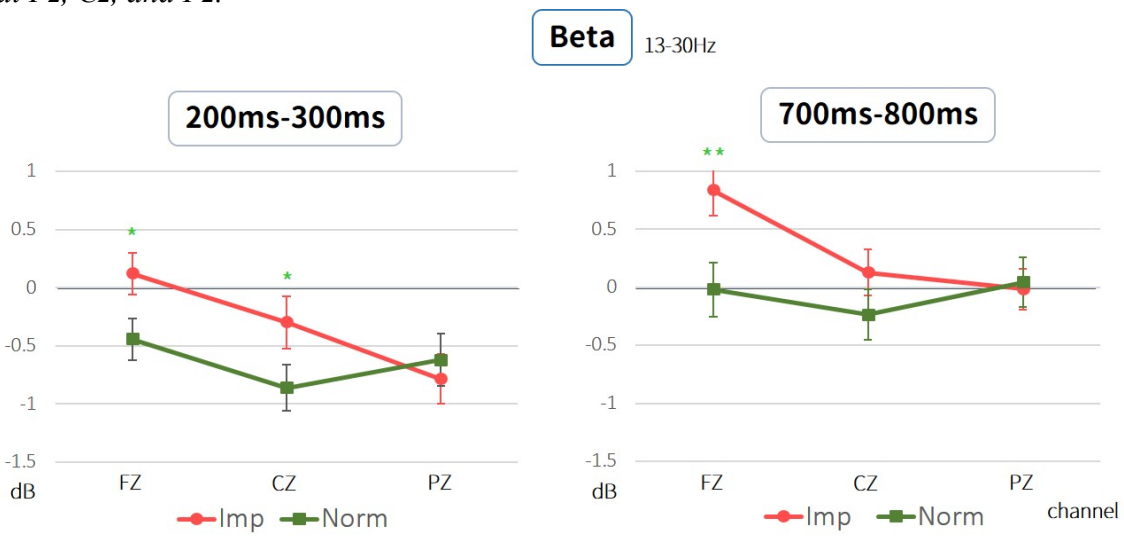

* $p < .05$. ** $p < .01$.

doi:10.6342/NTU202210143

Figure 7

The Perceptual Inference Task Behavioral Results.

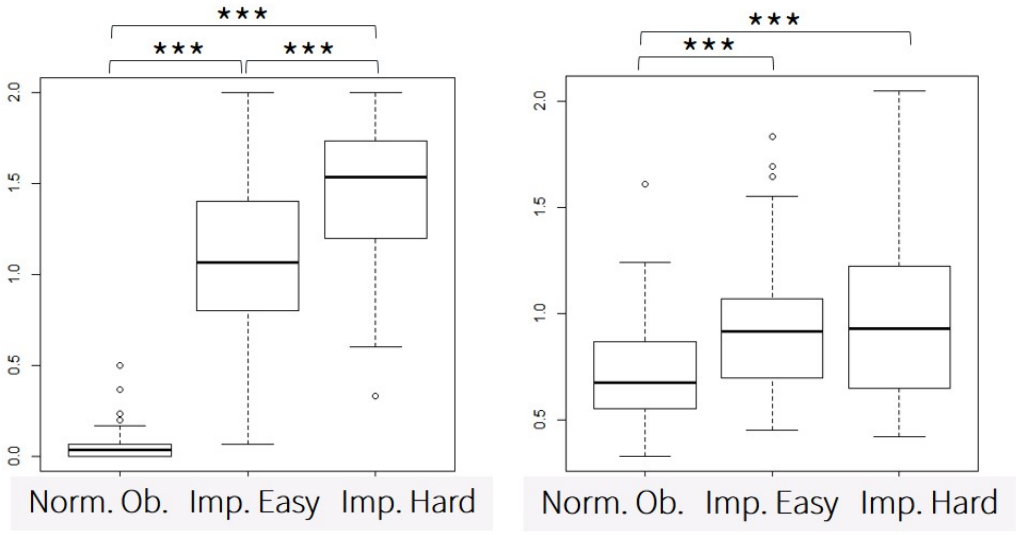

Note. The left figure is an accuracy, and the right figure is response time.
* $p < .05$. ** $p < .01$. *** $p < .001$.

doi:10.6342/NTU202210143

Figure 8

The Perceptual Inference Task First Rotation ERP Waveforms at Fz, Cz, and Pz.

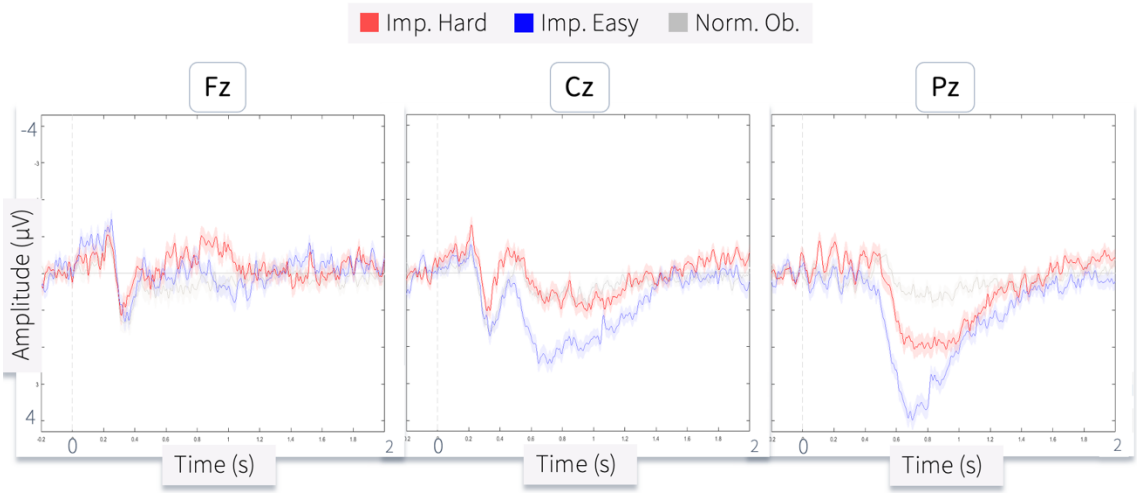

Figure 9

The Perceptual Inference Task Second Rotation ERP Waveforms at Fz, Cz, and Pz.

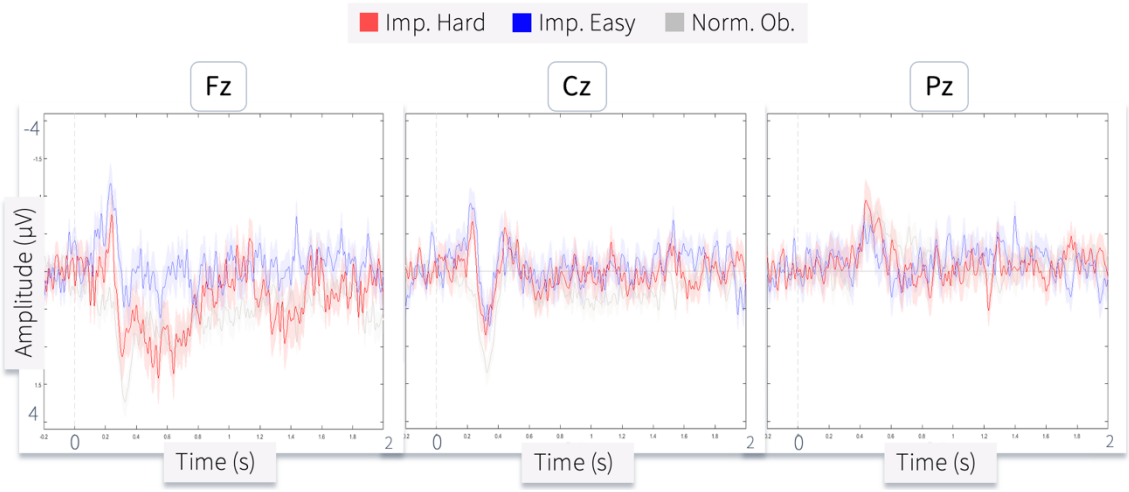

doi:10.6342/NTU202210143

Figure 10

The Perceptual Inference Task First Rotation ERP Post-hoc Results of 200-400 ms and 500-800 ms at Fz, Cz, and Pz.

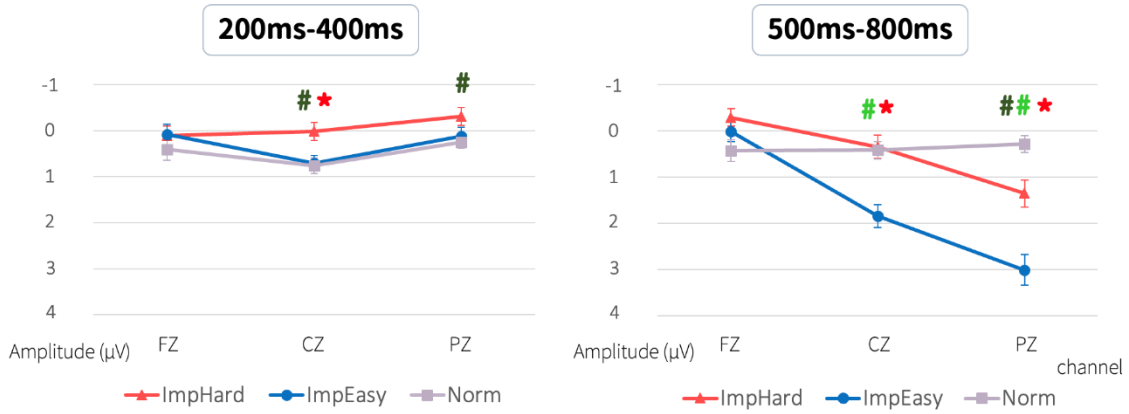

* $p < .05$. ** $p < .01$. *** $p < .001$.

Figure 11

The Perceptual Inference Task Second Rotation ERP Post-hoc Results of 200-400 ms and 500-800 ms at Fz, Cz, and Pz.

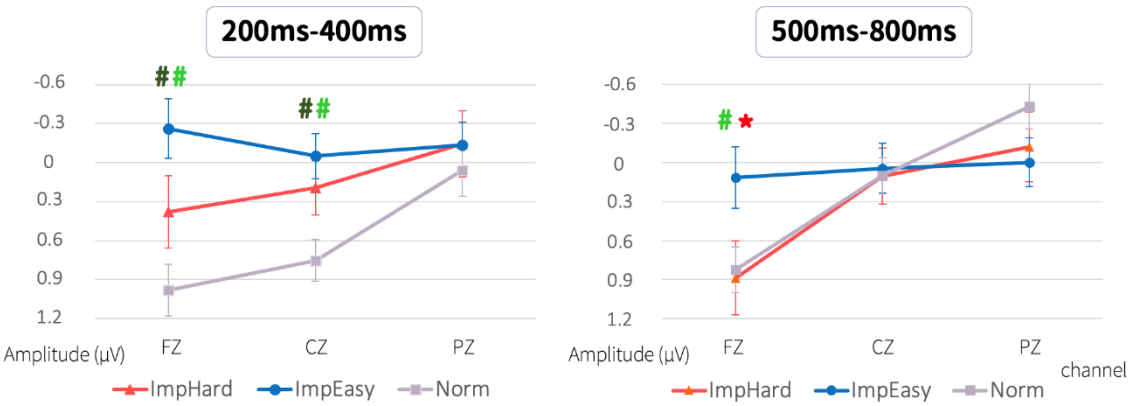

* $p < .05$. ** $p < .01$. *** $p < .001$.

doi:10.6342/NTU202210143

doi:10.6342/NTU202210143

Appendix A

Stimuli selection

Among all the third to sixth generations of 3D impossible objects designed by Kokichi Sugihara, we set to select 30 of them for the main experiment. We first chose a total of 54 objects from each category, including ambiguous cylinders, partly invisible objects, topology-disturbing objects, and deformable objects. The examples of the first selected 54 objects were shown in *Figure A1.1-1.4*. These 54 objects were then used in the preliminary experiment for the main stimuli selection. The experiment was designed to select 30 impossible objects that can be divided into three levels of configurational complexity. The results came out to be hard to choose ten objects for each level, we then decided to separate them into two levels instead. The details of this preliminary experiment will be described below.

Participants

Sixteen students of NTU participated in the preliminary experiment. The participants would gain extra points in General Psychology class. All participants agreed to take the task and signed the informed consent which follows ethical guidelines and is approved by the Institutional Review Board of the university.

Task Design

The task was designed as a spatial aptitude test, which is shown as in *Figure A2.1*. A picture of an object will be presented on the upper left side of the monitor, the two alternative perspectives of the object will also be presented on the lower left side of the monitor. The participants were introduced to imagine if there is a mirror behind the

doi:10.6342/NTU202210143

object, according to the upper left side picture, what they will see. The three options were presented side by side on the right side of the monitor. The participants were asked to give their answer by pressing the corresponding key of the one they think is the mirror image of the object.

There were two example trials at the start of the experiment for clarifying the procedure of the task. In these two examples, the answer will be given for the participants to fully understand the instruction (Figure A2.2 & A2.3). The additional seven trials were given without showing the answer for participants to get used to the task procedure. The impossible objects used in these seven practice trials were not included in the first selected 54 objects. These practice trials would not be included in the following analysis for selecting stimuli. After the practice trials, the formal task would begin. The objects were shown in random order, and each participant would see the different sequence of the objects. Participants' performance would be recorded, and their accuracy and response time of each object were used in selecting the formal stimuli for the main experiment.

Task Results

The results found it hard to branch out three complexity levels with 10 objects in each of it. We first chose the ten objects each with the highest, intermediate, and the lowest accuracy and/or with shorter, intermediate, and the longer response time, and further labeled them respectfully as the easy, medium, hard configuration level (the chosen 30 objects' average data was shown in *Table A1*). The middle class objects turned out to be hard to discriminate from the easy configuration level according to accuracy ($t(27) = 1.137$, $p = .5003$) (Table A2). Hence, we change to choose the 15

doi:10.6342/NTU202210143

objects with higher accuracy and/or shorter response time, and the 15 objects with lower accuracy and/or longer response time (Table A3). These respectfully constitute the two configuration complexity levels of the objects, the accuracy of two groups is significantly different (F (1, 28) = 182.9, $p < .001$) (Table A4). We also take the response time of recognizing each object into account. The response time of two levels showed a significant difference that the hard objects (more complex objects) take participants a slightly longer time to respond (the response time is adjusted within participants through minus the Median) (F (1, 15) = 5.453, $p < .05$) (Table A5).

Configuration Complexity Level Reassigned

According to the results above, the two levels of the objects were set (Table A6). We then 3D printed out all these 30 impossible objects and their corresponding regular objects, a total of 60 printed objects. Each object was then shot individually and carefully in a studio photoshoot light box, making sure that each object's different appearances can be correctly perceived. The video clips were shot and edited to match the specific timing for the main experiment, including 60 clips for the mirror task scenario and 60 clips for the inference scenario (Figure A3.1 & A3.2).

After the pilot study of the main experiments, the classification of configuration complexity levels were reassigned due to the difference of the task scenario. In the second part of the main experiment, the participants, the other 6 participants different from the 16 participants of the preliminary experiment of stimuli selection, were instructed to classify the configuration level of the objects through viewing the complete objects. The participants of the pilot study rated the complexity of the objects after watching the objects rotate two turns (720°). The results of this judgement were

doi:10.6342/NTU202210143

different from the preassigned stimuli levels (Table A7). The judgement scores for the preassigned stimuli levels were not significantly different (Table A8.1 & 8.2). As a result of this inconsistency, we conversely use the judgement score from these 6 participants to reassign the configuration complexity levels of existing 30 impossible objects (Table A9.1 & 9.2). This determination is given the perceptual inference task in the main experiment is more authentic, which presents the real objects with a multi-angle view of them. The final two configuration complexity levels, hard and easy level, of the objects were listed in *Table A10* (also the figures of the objects). This final grouping would be fixed throughout the following experiment.

doi:10.6342/NTU202210143

Figure A

Figure A1.1
Examples of the First Selected 54 Objects from Each Category. Ambiguous cylinders: Full Moon and Hexagonal Star.

Direct View Alternative View

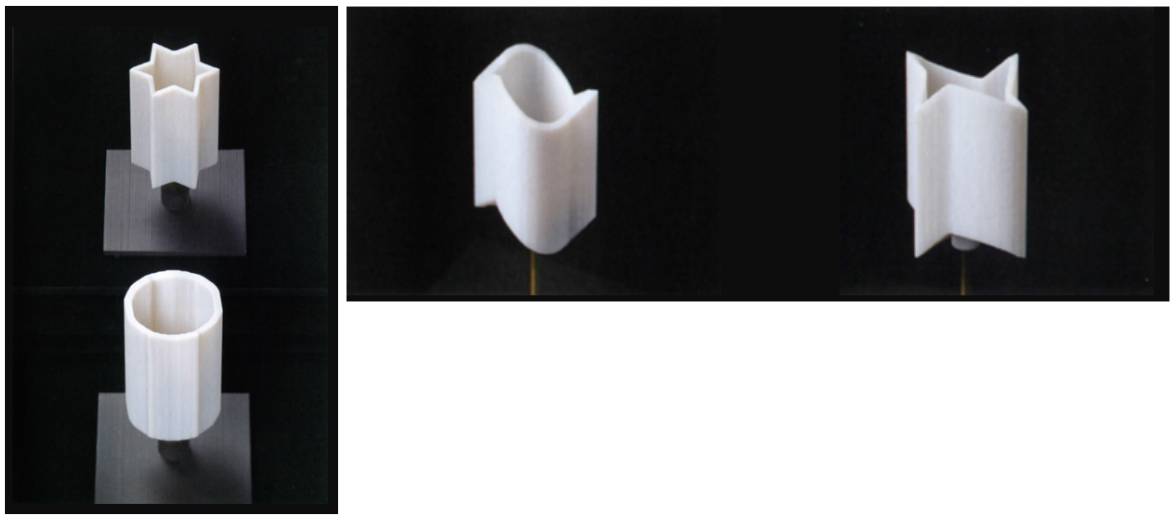

Figure A1.2
Examples of the First Selected 54 Objects from Each Category. Partly invisible objects: Hide of a Circle 1.

Direct View Alternative View

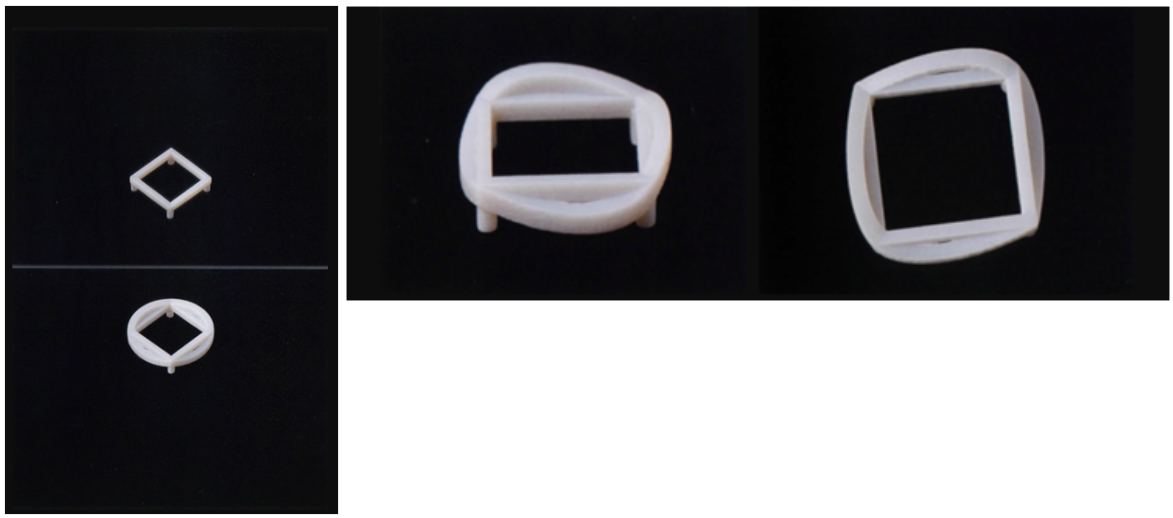

doi:10.6342/NTU202210143

Figure A1.3

*Examples of the First Selected 54 Objects from Each Category.*Topology-disturbing objects: Cylinder and two Parallel Walls.

Direct View Alternative View

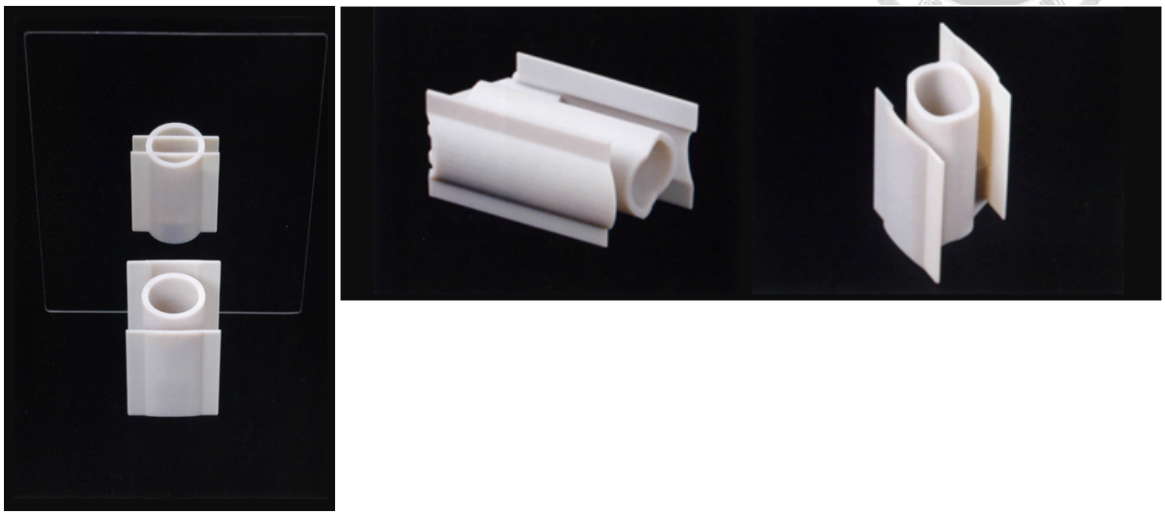

Figure A1.4

Examples of the First Selected 54 Objects from Each Category. Deformable objects: Six-petal Flower and Butterfly.

Direct View Alternative View

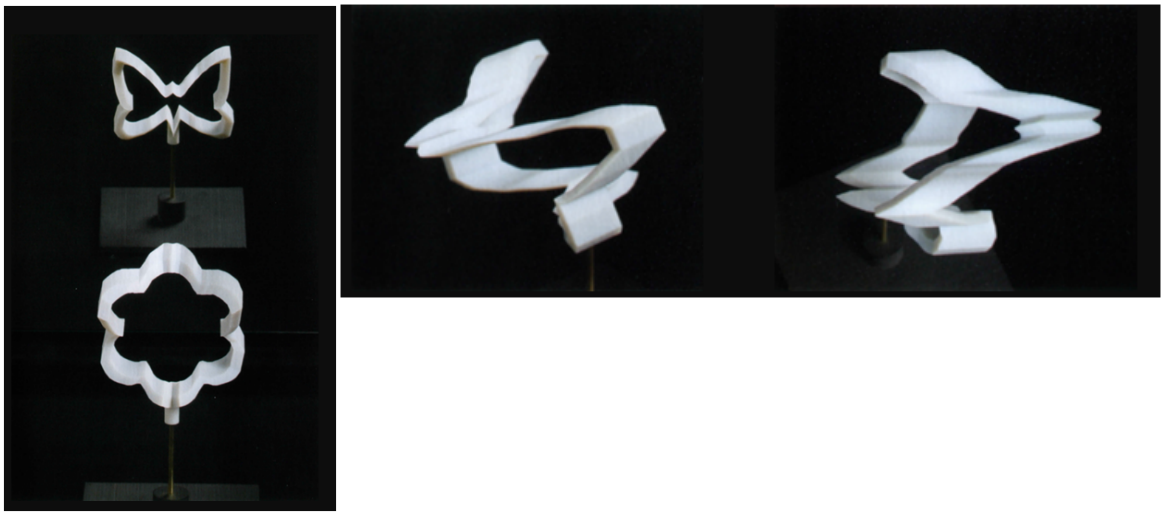

doi:10.6342/NTU202210143

Figure A2.1
Task Design of Stimuli Selection: Instruction.

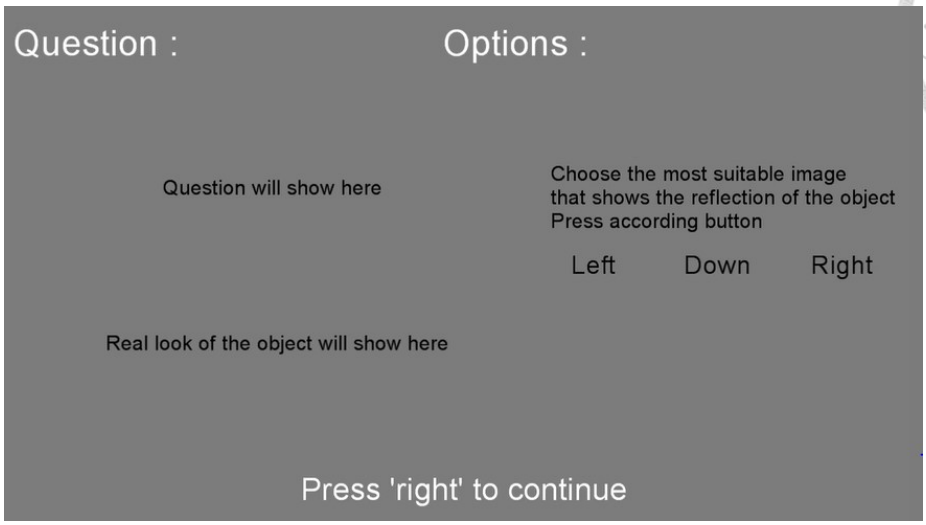

Figure A2.2
Task Design of Stimuli Selection: Example trial.

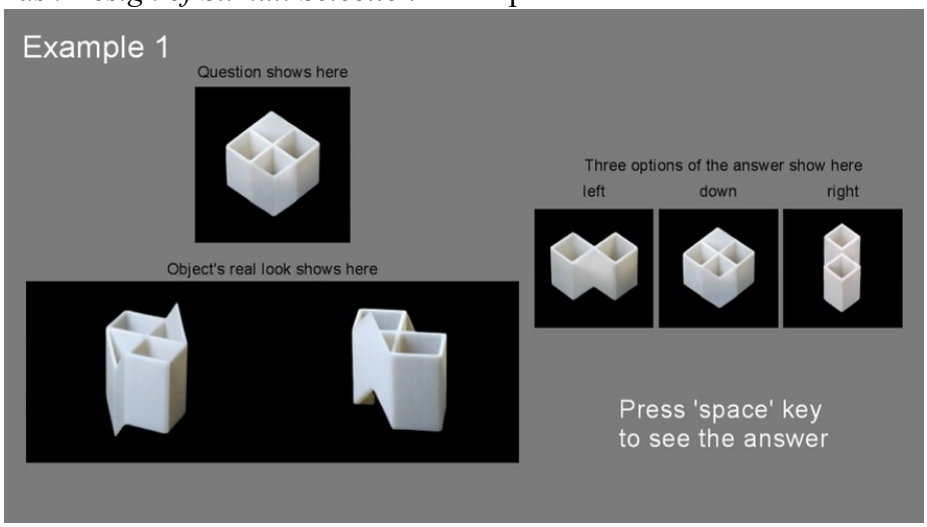

Figure A2.3
Task Design of Stimuli Selection: Answer of the example trial.

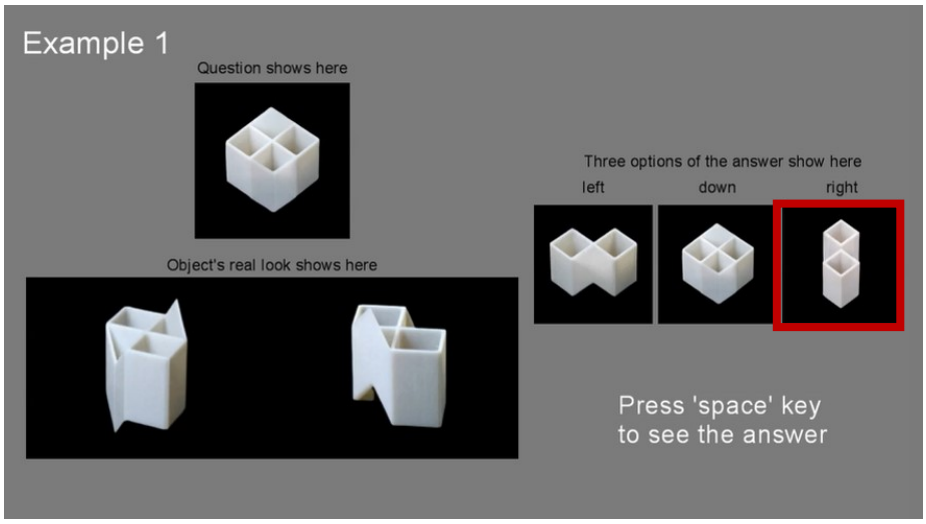

doi:10.6342/NTU202210143

Figure A3.1
Main Experiment Video Clips Screenshot Example: Mirror task scenario.

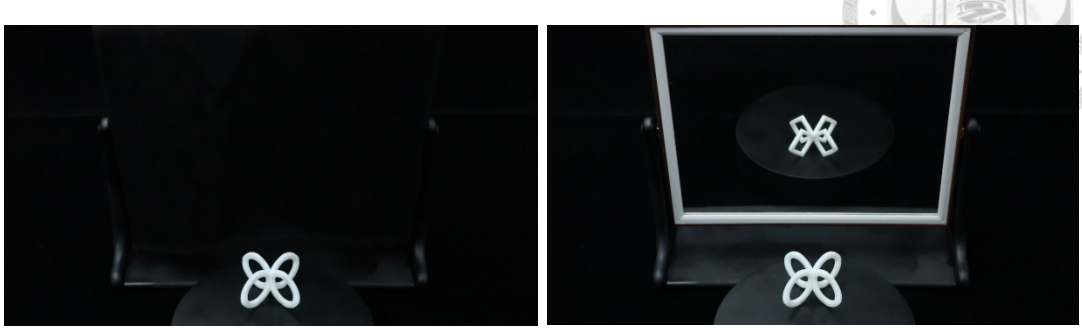

Note. Video timeline: left: 0-3000 ms; right: 3500-6500 ms

Figure A3.2
Main Experiment Video Clips Screenshot Example: Inference scenario.

Note. Video timeline: left: 0-1500 ms; middle: 3500-5000 ms; right: 7000-8500 ms

doi:10.6342/NTU202210143

Table A

Table A1

The First Labeled Objects of the Easy, Medium, Hard Configuration Levels

Configuration Level	Accuracy		Response Time	
	M (%)	*SD*	*M* (s)	*SD*
Easy	66.89	0.1933	27.456	7.124
Medium	58.75	0.1698	34.292	6.243
Hard	37.5	0.1021	36.253	10.339

Table A2.1

One way ANOVA Result of First Labeled Configuration Level: Accuracy

Source	*df*	*SS*	*MS*	*F*	*p*
Configuration Levels	2	0.4602	0.23008	9.01	0.00101**
Residuals	27	0.6895	0.02554		

Table A2.2

Multiple Comparison of First Labeled Configuration Level: Accuracy

Contrast	*estimate*	*SE*	*df*	*t*	*p*
Easy-Hard	0.2938	0.0715	27	4.110	0.0009***
Easy-Medium	0.0813	0.0715	27	1.137	0.5003
Hard-Medium	-0.2125	0.0715	27	-2.974	0.0163**

doi:10.6342/NTU202210143

Table A3

Adjusted Easy and Hard Configuration Level

Configuration Level	Accuracy		Response Time	
	M (%)	*SD*	*M* (s)	*SD*
Easy	73.33	0.0727	28.637	7.213
Hard	35.42	0.0807	33.843	9.009

Table A4

ANOVA Result of Adjusted Easy and Hard Configuration Level: Accuracy

Source	*df*	*SS*	*MS*	*F*	*p*
Configuration Levels	1	1.0783	1.0783	182.9	< 0.001***
Residuals	28	0.1651	0.0059		

Table A5

Repeated Measure ANOVA Result of Adjusted Easy and Hard Configuration Level: Response time

Source	df_{num}	*SS*	*dfden*	SS_{Error}	*F*	*p*
(Intercept)	1	31229.8	15	6503.7	72.0279	< 0.001***
Configuration Levels	1	216.8	15	596.4	5.4527	0.0339**

doi:10.6342/NTU202210143

Table A6
List of Two Configuration Level Impossible Objects

	Easy	Hard
1	Circle and Triangle	Crossing Circular Cylinders and Separated Rectangular Cylinders
2	Crescent and Star	Bat Under a Full Moon
3	Diamond and Spade	Circle and Square
4	Heart and Spade	Diamond and Club
5	Triangle and Rectangle	Heart and Club
6	Triangle and Star	Heart and Diamond
7	Slanted Parade of Cylinders	Rectangle and Star
8	Ring Sinking into the Desk Surface 1	Six-petal Flower and Butterfly
9	Partly Invisible Square Cylinders	Separation of Co-centric Circles Penetrated by a Wall
10	Four-Petal Flower	Vertically Aligned Crossing Rectangular Cylinders
11	Falk Dance of Five Circular Rectangles	Hide of a Circle 1
12	Bat and Star	Desire of Cylinders Toward Secret Meeting
13	Crescent and Star (Cylinders)	Hide of a Star
14	Secret Meeting of Circular Cylinders	Full Moon and Hexagonal Star
15	Rectangle and Hexagonal Star	Translation of a Crescent

doi:10.6342/NTU202210143

Table A7

Judgement Score of the Pilot Study

Objects	Participants						
	1	2	3	4	5	6	Mean
Impossible Objects							
Easy	1.27	1.53	1.20	1.47	0.93	1.00	1.23
Hard	1.27	1.60	1.27	1.20	1.00	1.07	1.23
Normal Objects	0	0	0.03	0	0	0	0.01

Table A8.1

One way ANOVA Result of Judgement Score of the Pilot Study

Source	*df*	*SS*	*MS*	*F*	*p*
Configuration Levels	2	135.67	67.83	330.9	<0.001***
Residuals	357	73.19	0.21		

Table A8.2

Multiple Comparison of Judgement Score of the Pilot Study

Contrast	*estimate*	*df*	*t*	*p*
Easy-Hard	0.00	357	0.000	1
Easy-Normal	1.23	357	21.003	<0.001***
Hard-Normal	1.23	357	21.003	<0.001***

doi:10.6342/NTU202210143

Table A9.1

One way ANOVA Result of Reassigned Judgement Score of the Pilot Study

Source	*df*	*SS*	*MS*	*F*	*p*
Configuration Levels	2	158.43	79.21	560.66	<0.001***
Residuals	357	50.44	0.14		

Table A9.2

Multiple Comparison of Reassigned Judgement Score of the Pilot Study

Contrast	*estimate*	*df*	*t*	*p*
Easy-Hard	0.71	357	12.69	<0.001***
Easy-Normal	0.88	357	17.97	<0.001***
Hard-Normal	1.59	357	32.629	<0.001***

doi:10.6342/NTU202210143

Table A10

List and Figures of Two Configuration Level Objects (reassigned objects are colored in red)

	Easy		Hard	
1	Circle and Triangle	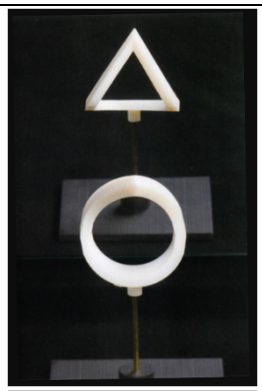	Crossing Circular Cylinders and Separated Rectangular Cylinders	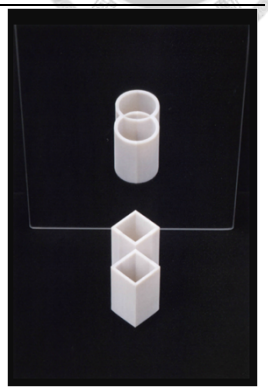
2	Bat Under a Full Moon		Crescent and Star	
3	Diamond and Spade	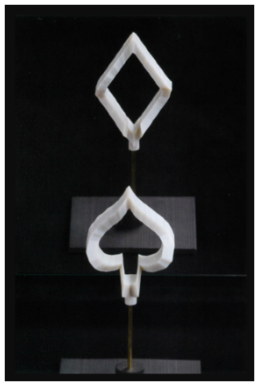	Slanted Parade of Cylinders	
4	Heart and Spade	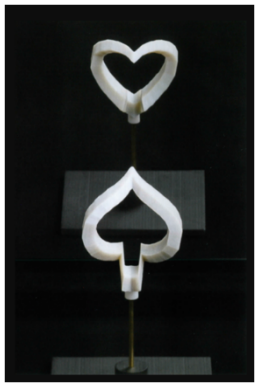	Diamond and Club	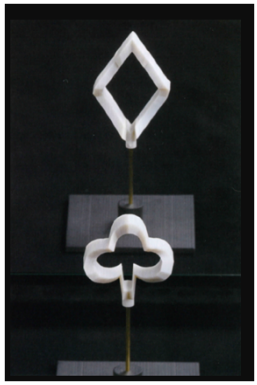

doi:10.6342/NTU202210143

Table A10

List and Figures of Two Configuration Level Objects (reassigned objects are colored in red) (continued)

	Easy		Hard	
5	Triangle and Rectangle	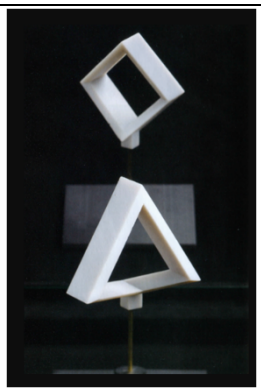	Four-Petal Flower	
6	Triangle and Star	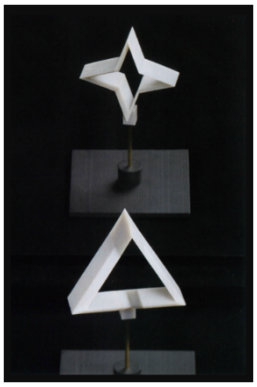	Falk Dance of Five Circular Rectangles	
7	Circle and Square		Rectangle and Star	
8	Ring Sinking into the Desk Surface 1		Six-petal Flower and Butterfly	

doi:10.6342/NTU202210143

Table A10

List and Figures of Two Configuration Level Objects (reassigned objects are colored in red) (continued)

	Easy		Hard	
9	Partly Invisible Square Cylinders	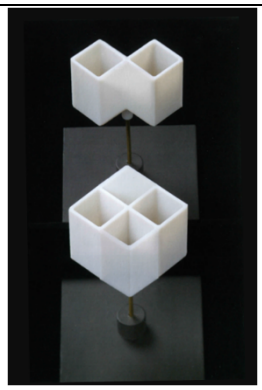	Separation of Co-centric Circles Penetrated by a Wall	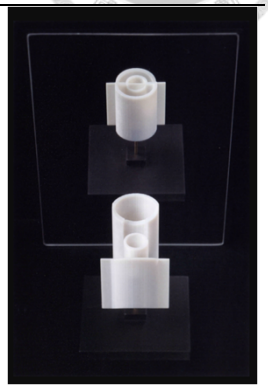
10	Heart and Club	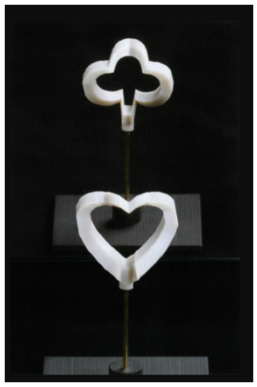	Bat and Star	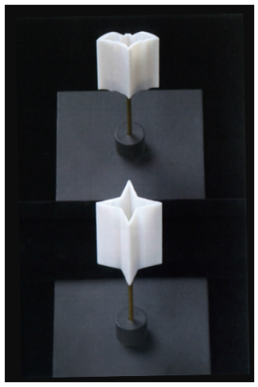
11	Heart and Diamond Cylinders		Hide of a Circle 1	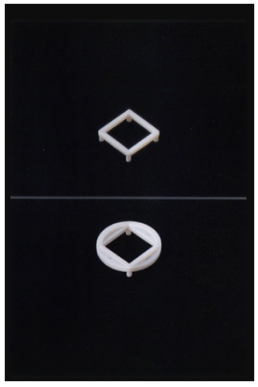
12	Vertically Aligned Crossing Rectangular	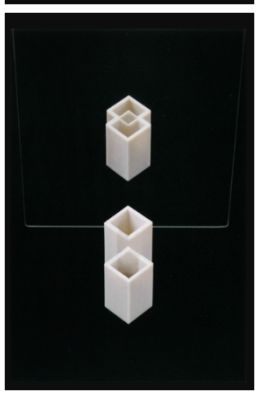	Crescent and Star (Cylinders)	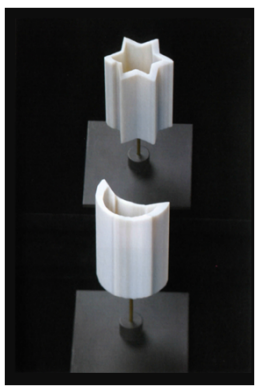

doi:10.6342/NTU202210143

Table A10

List and Figures of Two Configuration Level Objects (reassigned objects are colored in red) (continued)

	Easy		Hard	
13	Desire of Cylinders Toward Secret Meeting		Hide of a Star	
14	Secret Meeting of Circular Cylinders	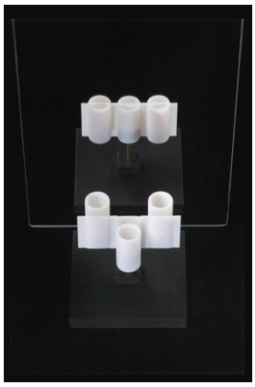	Full Moon and Hexagonal Star	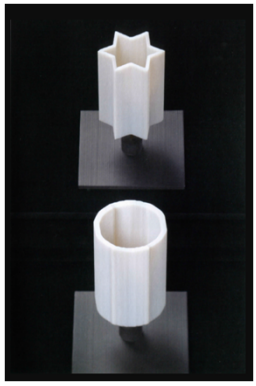
15	Translation of a Crescent	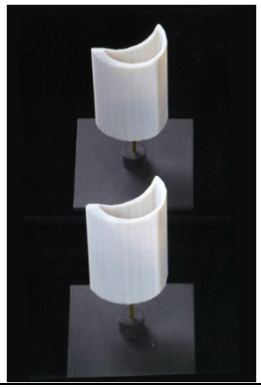	Rectangle and Hexagonal Star	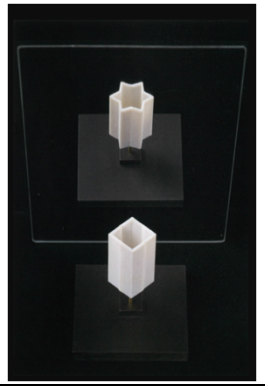

doi:10.6342/NTU202210143

doi:10.6342/NTU202210143

Appendix B

Figure B

Figure B1

The Peekaboo Task ERP Waveforms at Six Midline Channels.

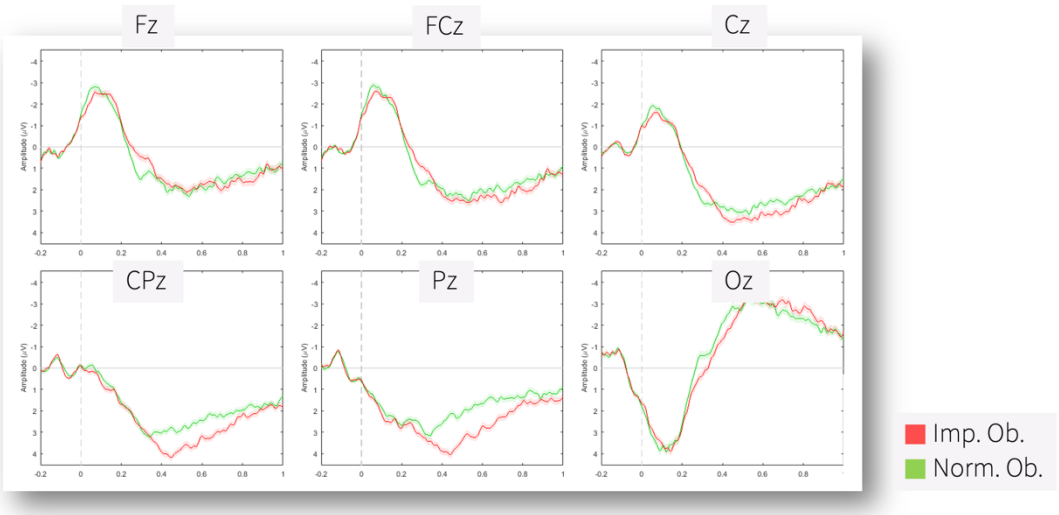

doi:10.6342/NTU202210143

Figure B2.1

The Peekaboo Task ERSP Heat Map at FCz.

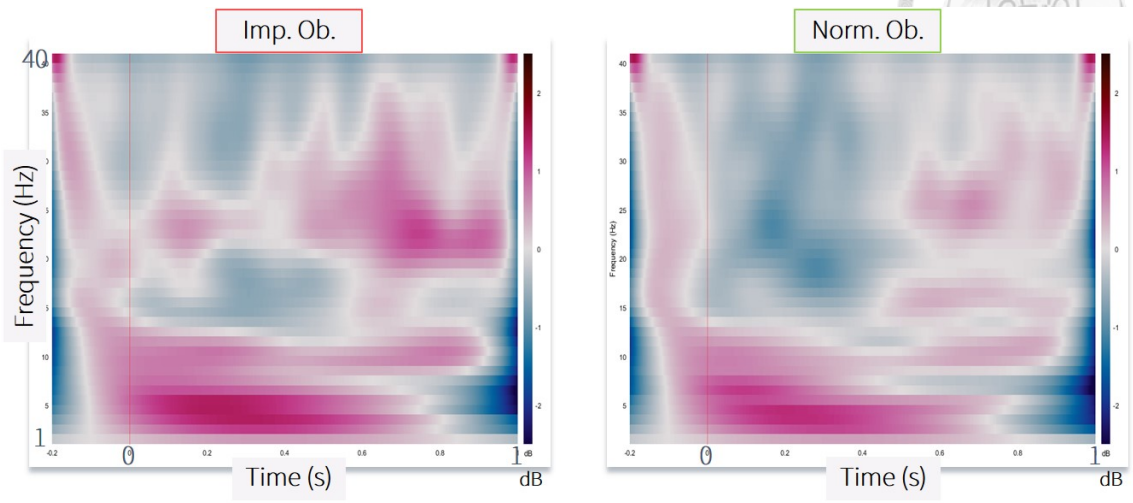

Figure B2.2

The Peekaboo Task ERSP Heat Map at CPz.

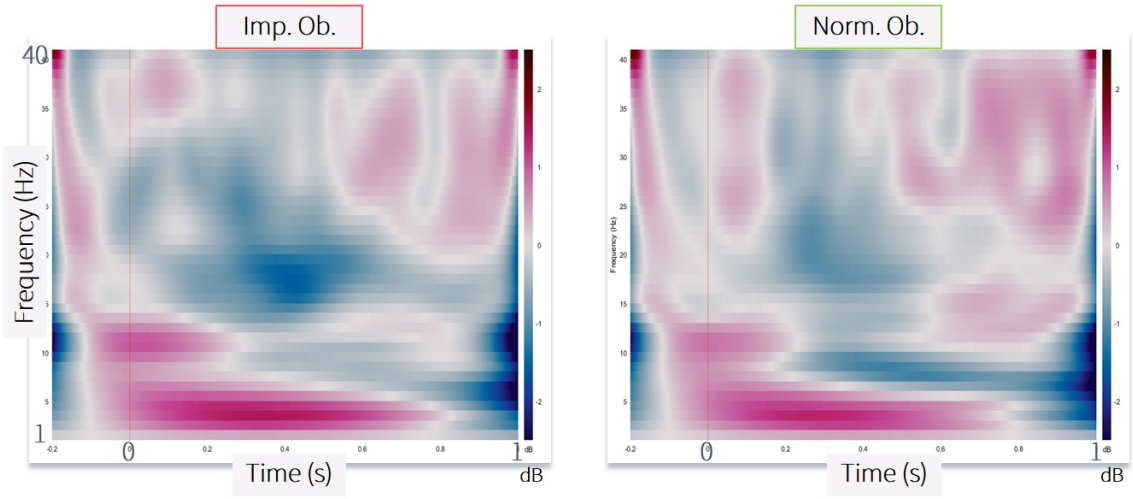

Figure B2.3

The Peekaboo Task ERSP Heat Map at Oz.

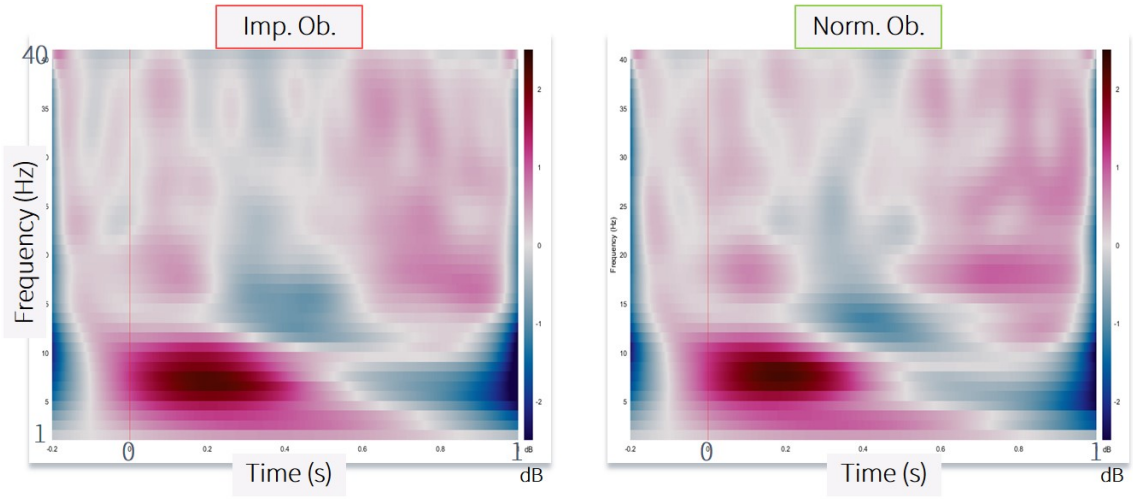

doi:10.6342/NTU202210143

Figure B3

The Perceptual Inference Task MVPA Results of the First Rotation.

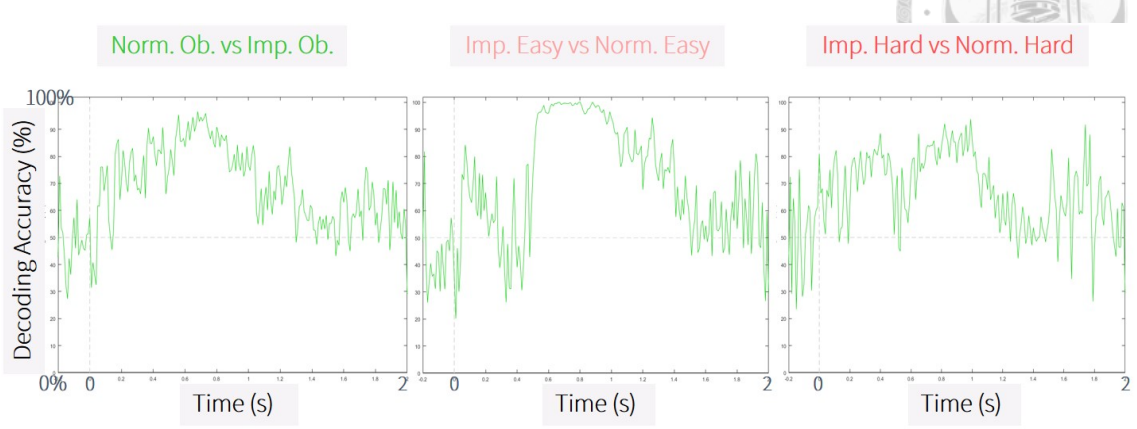

Figure B4

The Perceptual Inference Task MVPA Results of the Second Rotation.

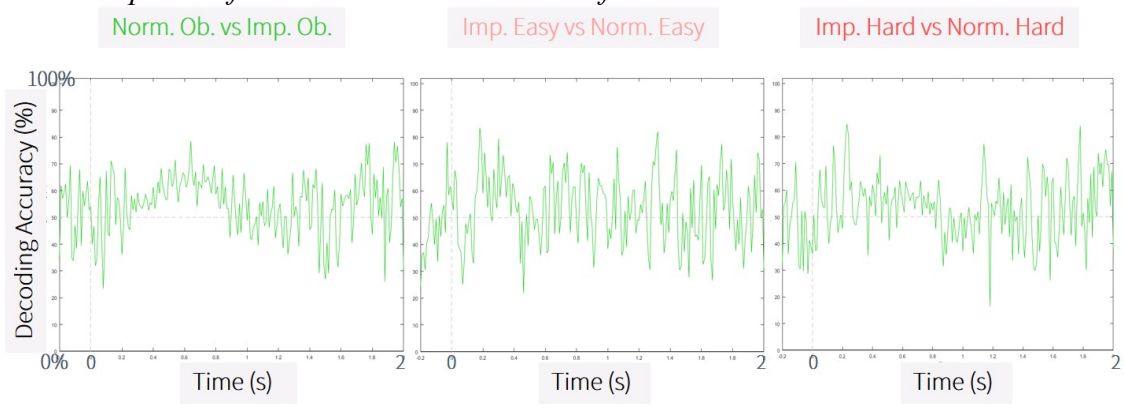

doi:10.6342/NTU202210143

Figure B5

The Perceptual Inference Task ERP Waveforms of the First Rotation at Six Midline Channels.

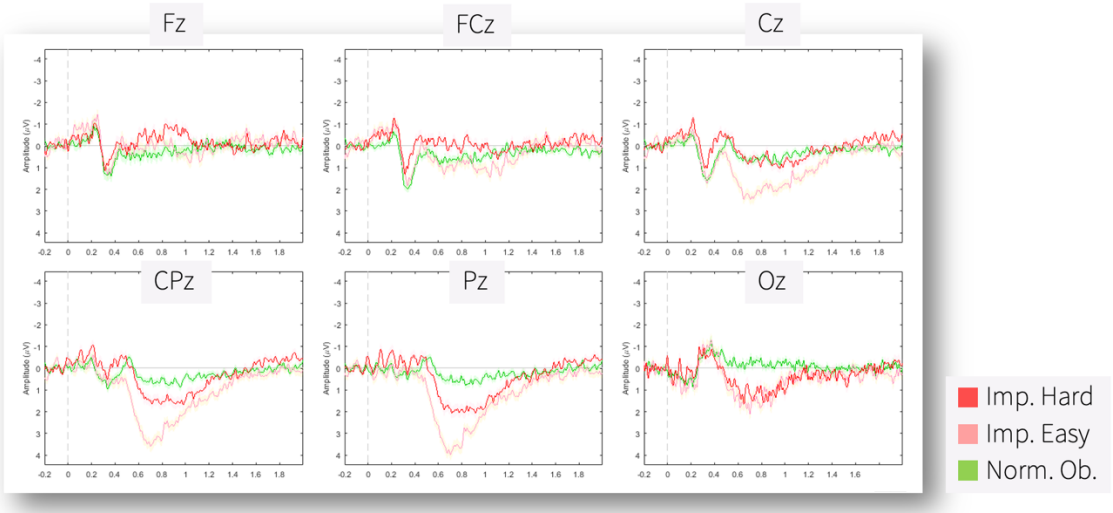

Figure B6

The Perceptual Inference Task ERP Waveforms of the Second Rotation at Six Midline Channels.

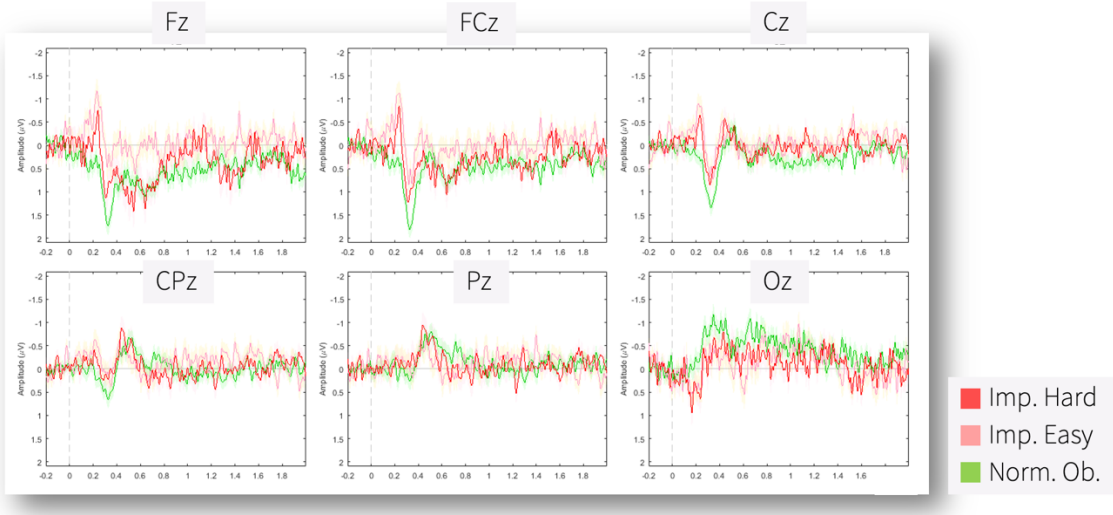

doi:10.6342/NTU202210143

Figure B7

The Perceptual Inference Task ERP Waveforms of the First Stop at Six Midline Channels.

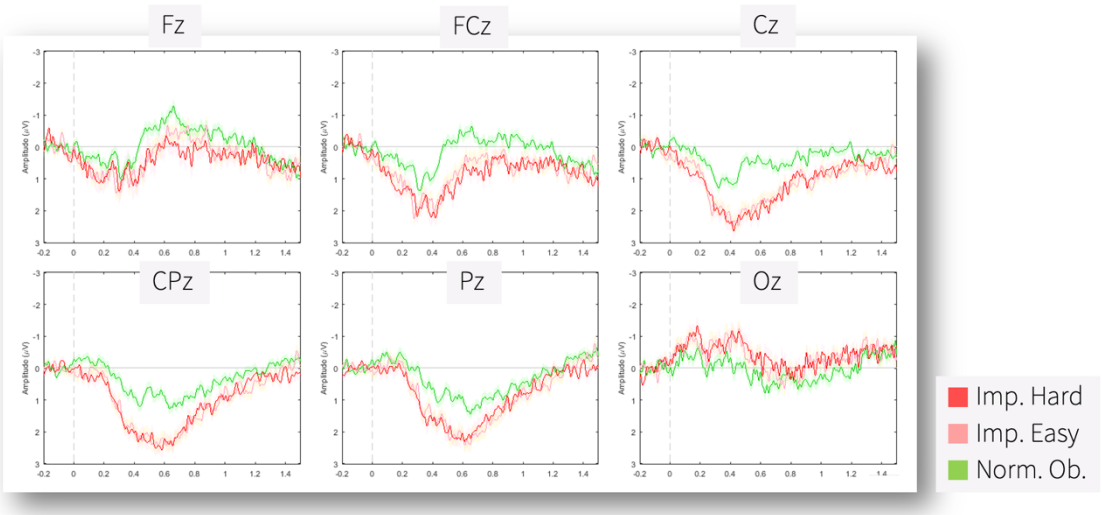

Figure B8

The Perceptual Inference Task ERP Waveforms of the Second Stop at Six Midline Channels.

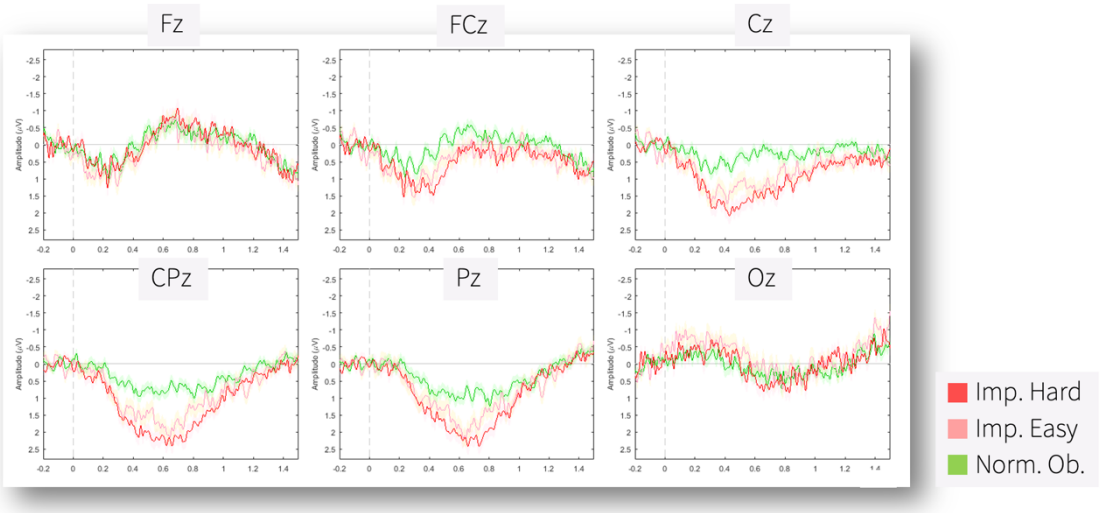

doi:10.6342/NTU202210143

Figure B9

The Perceptual Inference Task ERP Waveforms of the Third Rotation at Six Midline Channels.

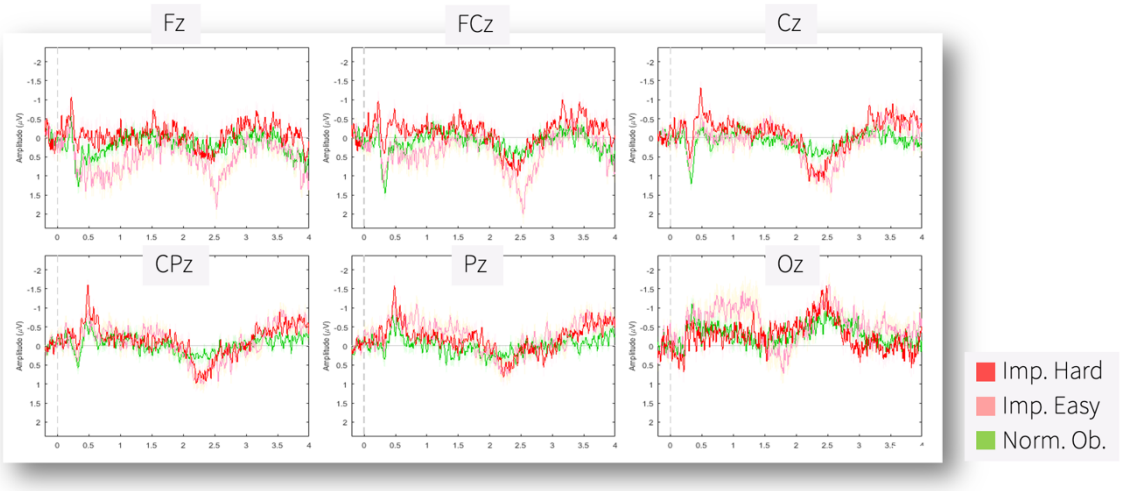

doi:10.6342/NTU202210143

Table B

Table B1

RM-ANOVA Results of the Peekaboo Task's Behavior Performance: Accuracy

Predictor	df_{Num}	SS_{Num}	df_{Den}	SS_{Den}	F	p
Configuration Levels	2	0.002	74	0.124	0.564	0.571

Table B2

RM-ANOVA Results of the Peekaboo Task's Behavior Performance: Response time

Predictor	df_{Num}	SS_{Num}	df_{Den}	SS_{Den}	F	p
Configuration Levels	2	0.012	74	0.429	1.030	0.362

Table B3

RM-ANOVA Results of the Peekaboo Task's ERP 200-300 ms

Predictor	df_{Num}	SS_{Num}	df_{Den}	SS_{Den}	F	p
Channel	5	$3.86e^{-10}$	155	$1.32e^{-09}$	9.051	$1.44\ e^{-07}$ ***
Object	1	$1.36e^{-11}$	31	$9.40e^{-11}$	4.469	0.043 **
Channel x Object	5	$3.75e^{-11}$	155	$3.92e^{-10}$	2.968	0.014 *

Note. * $p < .05$. ** $p < .01$. *** $p < .001$.

Table B4

RM-ANOVA Results of the Peekaboo Task's ERP 800-900 ms

Predictor	df_{Num}	SS_{Num}	df_{Den}	SS_{Den}	F	p
Channel	5	$6.18e^{-10}$	155	$1.20e^{-09}$	15.923	$1.21\ e^{-12}$ ***
Object	1	$1.28e^{-11}$	31	$8.50e^{-11}$	4.680	0.038 *
Channel x Object	5	$4.13e^{-11}$	155	$3.66e^{-10}$	3.503	0.005 **

Note. * $p < .05$. ** $p < .01$. *** $p < .001$.

doi:10.6342/NTU202210143

Table B5

RM-ANOVA Results of the Peekaboo Task's ERSP 400-500 ms of Delta Band

Predictor	df_{Num}	SS_{Num}	df_{Den}	SS_{Den}	F	p
Channel	5	1.309	155	41.573	0.976	0.435
Object	1	2.518	31	12.640	6.175	0.019 *
Channel x Object	5	0.758	155	21.995	1.069	0.005

Note. * $p < .05$.

Table B6

RM-ANOVA Results of the Peekaboo Task's ERSP 400-500 ms of Theta Band

Predictor	df_{Num}	SS_{Num}	df_{Den}	SS_{Den}	F	p
Channel	5	27.425	155	199.453	3.263	0.001 **
Object	1	21.520	31	54.919	12.147	0.002 **
Channel x Object	5	6.059	155	132.207	1.421	0.220

Note. * $p < .05$. ** $p < .01$.

Table B7

RM-ANOVA Results of the Peekaboo Task's ERSP 400-500 ms of Alpha Band

Predictor	df_{Num}	SS_{Num}	df_{Den}	SS_{Den}	F	p
Channel	5	33.107	155	218.19	4.704	.0005 ***
Object	1	34.197	31	86.78	12.217	.0015 **
Channel x Object	5	2.156	155	282.48	0.237	.9459

Note. * $p < .05$. ** $p < .01$. *** $p < .001$.

doi:10.6342/NTU202210143

Table B8

RM-ANOVA Results of the Peekaboo Task's ERSP 200-300 ms of Beta band

Predictor	df_{Num}	SS_{Num}	df_{Den}	SS_{Den}	F	p
Channel	5	13.930	155	113.492	3.805	.0028 **
Object	1	6.959	31	98.249	2.196	.1485
Channel x Object	5	11.634	155	101.495	3.553	.0045 **

Note. * $p < .05$. ** $p < .01$.

Table B9

RM-ANOVA Results of the Peekaboo Task's ERSP 700-800 ms of Beta Band

Predictor	df_{Num}	SS_{Num}	df_{Den}	SS_{Den}	F	p
Channel	5	15.704	155	151.91	3.205	.0088 **
Object	1	9.120	31	103.05	2.744	.1077
Channel x Object	5	14.930	155	120.07	3.855	.0026 **

Note. * $p < .05$. ** $p < .01$.

doi:10.6342/NTU202210143

Table B10

RM-ANOVA Results of the Perceptual Inference Task's Behavior Performance: Subjective Configuration Score

Predictor	df_{Num}	SS_{Num}	df_{Den}	SS_{Den}	F	p
Configuration Levels	2	39.677	74	4.245	345.85	$< 2.2e^{-16}$ ***

Note. *** $p < .001$.

Table B11

RM-ANOVA Results of the Perceptual Inference Task's Behavior Performance: Response Time

Predictor	df_{Num}	SS_{Num}	df_{Den}	SS_{Den}	F	p
Configuration Levels	2	1.628	74	3.620	16.637	$1.08e^{-06}$ ***

Note. *** $p < .001$.

Table B12

RM-ANOVA Results of the Perceptual Inference Task's First Rotation ERP 200-400 ms

Predictor	df_{Num}	SS_{Num}	df_{Den}	SS_{Den}	F	p
Channel	5	$5.54e^{-11}$	175	$3.89e^{-10}$	4.983	.0003 ***
Object	2	$2.96e^{-11}$	70	$1.28e^{-10}$	8.066	.0007 ***
Channel x Object	10	$1.15e^{-11}$	350	$2.45e^{-10}$	1.640	.094 #

Note. # $p < 0.1$. * $p < .05$. ** $p < .01$. *** $p < .001$.

Table B13

RM-ANOVA Results of the Perceptual Inference Task's First Rotation ERP 500-800 ms

Predictor	df_{Num}	SS_{Num}	df_{Den}	SS_{Den}	F	p
Channel	5	$1.71e^{-10}$	175	$4.72e^{-10}$	12.720	$1.50e^{-10}$ ***
Object	2	$2.22e^{-10}$	70	$2.15e^{-10}$	36.065	$1.72e^{-11}$ ***
Channel x Object	10	$1.56e^{-10}$	350	$3.00e^{-10}$	18.198	$< 2.2e^{-16}$ ***

Note. *** $p < .001$.

doi:10.6342/NTU202210143

Table B14

RM-ANOVA Results of the Perceptual Inference Task's Second Rotation ERP 200-400 ms

Predictor	df_{Num}	SS_{Num}	df_{Den}	SS_{Den}	F	p
Channel	5	$4.38e^{-11}$	175	$3.55e^{-10}$	4.317	.00099 ***
Object	2	$3.13e^{-11}$	70	$1.87e^{-10}$	5.853	.00446 **
Channel x Object	10	$4.55e^{-11}$	350	$3.11e^{-10}$	5.108	$5.67e^{-07}$ ***

Note. ** $p < .01$. *** $p < .001$.

Table B15

RM-ANOVA Results of the Perceptual Inference Task's Second Rotation ERP 500-800 ms

Predictor	df_{Num}	SS_{Num}	df_{Den}	SS_{Den}	F	p
Channel	5	$7.62e^{-11}$	175	$3.83e^{-10}$	6.953	$6.01e^{-06}$ ***
Object	2	$4.25e^{-12}$	70	$2.14e^{-10}$	0.696	0.502
Channel x Object	10	$2.39e^{-11}$	350	$3.18e^{-10}$	2.632	0.004 **

Note. ** $p < .01$. *** $p < .001$.

doi:10.6342/NTU202210143